1-1-2014

Miniature Printed Antennas and Filters Using Volumetric Reactive Pins and Lumped Circuit Loadings

Saurabh Gupta
University of South Florida, saurabhgupta@mail.usf.edu

Miniature Printed Antennas and Filters Using Volumetric Reactive Pins and Lumped Circuit Loadings

by

Saurabh Gupta

A dissertation submitted in partial fulfillment
of the requirements for the degree of
Doctor of Philosophy in Electrical Engineering
Department of Electrical Engineering
College of Engineering
University of South Florida

Major Professor: Gokhan Mumcu, Ph.D.
Thomas Weller, Ph.D.
Lawrence Dunleavy, Ph.D.
Nathan Crane, Ph.D.
Paul A. Herzig, B.S.E.E.

Date of Approval:
November 5, 2014

Keywords: GPS, Circular Polarization, Volumetric Loading,
Filter, Mutual Coupling

DEDICATION

To my dear parents: Dr. Vinod Kumar Gupta and Dr. Shashi Kanti Gupta, my lovely beautiful sisters: Manisha, Swati and Smita, my brother-in-laws: Sudhir Kumar Bagga and Dr. Mayank Devangan; my nephews and nieces: Arpita, Abhishek, Sakshi, Abhiraj and Jiya. Lastly, to the almighty and my late. Guru (Godavari Giri Ji Maharaj).

ACKNOWLEDGMENTS

I would like to express my deepest gratitude to my advisor Dr. Gokhan Mumcu for his consistent support, guidance and help through my doctoral studies. This would have not been possible without his excellent and in depth knowledge in the areas of electromagnetics, microwave and antennas that provided me with a clear path to reach my research goals. Being his first student, I was fortunate to obtain his direct guidance and hands on experience. It was my privilege and honor to be a part of his research group.

I am sincerely thankful to Dr. Thomas Weller, Dr. Lawrence Dunleavy, Dr. Nathan Crane and Paul A. Herzig for being a part of my PhD. committee and providing me with their valuable suggestions and comments. I would like to thank Paul for providing and letting me to be a part of a project which contributed a lot to my research. A special thanks to Dr. Dunleavy for being a supportive course instructor which later proved to be a back bone for my theoretical knowledge. Also, I am thankful to him for providing me with mine first industrial experience as an intern at Modelithics Inc.

I would like to thank my colleagues in the WAMI group: Bojana, David, Sergio, Ibrahim, Tony, Quenton, Olawale, Maria, Michael, Timothy, Abhishek, Patrick, Anand for their help and support. A special thanks to Ahmad Gheethan, Ankush, Shakeel, Salman and Feroz for being supporting friends and a helpful hand whenever needed.

I want to thank all teachers from my school and undergrad for their effort in educating me with basic yet pivotal knowledge. A special thanks to Kamran Cheema, Alberto Canabal and

Pierre Girard for being wonderful bosses at TDK-EPCOS and helping me in finishing my dissertation.

I would like to thank my family, especially my parents, for the kind of help and support they have given me to achieve this mile stone. There are no words that I can use to express my gratitude to them for keeping their faith and encouraging me at the times when I needed it the most. Lastly, I would like to thank the almighty and my late Guru for his blessings without which this journey would have never been possible.

TABLE OF CONTENTS

LIST OF TABLES

LIST OF FIGURES

ABSTRACT

This dissertation presents a new technique for miniaturization of printed RF circuits and antennas. The technique is based on lumped circuit elements and volumetric reactive pin loadings. The vertical arrangement of the pins is shown to provide a meandered current path within the device volume enhancing the miniaturization achieved with sole application of lumped circuit components. The technique is applied for antenna and filter size reduction. In antenna applications, it is shown that due to the presence of the reactive pin loading the overall size of a printed antenna can be miniaturized without affecting the radiation efficiency performance. One of the major advantages of this approach over the existing miniaturization techniques is that it allows reducing the overall size of the antenna (i.e. the substrate size) in addition to its metallization footprint area. Specifically, three antenna designs are presented for GPS and ISM applications. Firstly, a miniaturized wide-band CDL antenna has been introduced. The antenna consists of two loops which are loaded with lumped inductors and coupling capacitors. The design is shown to exhibits 49% smaller footprint size as compared to a traditional patch antenna without degrading the bandwidth performance. Secondly, a circular polarized compact dual-band CDL GPS antenna loaded with lumped capacitors and vertical pins is shown. The antenna operates with >50% lesser area as compared to a traditional L2 patch antenna without degrading its radiation performance. Thirdly, a patch antenna with its cavity loaded with CSRRs is presented. The novelty of the design is that it provides circularly

symmetric arrangement of CSRRs thereby enabling the antenna to exhibit circular polarization (CP). Apart from CSRR, further size reduction is obtained by simultaneously reducing the substrate size and ground plane metallization around the CSRRs and loading it with pins. The antenna is 44% smaller than a traditional patch antenna without causing degradation in the antenna's radiation efficiency performance. To extend the volumetric loading to filter applications, the last chapter of the dissertation presents a detailed analysis to understand how geometrical factors (e.g. periodicity, radius, width of the host transmission line, etc) affect the miniaturization performance and quality factor. As a design example, a 2GHz pin loaded hairline filter with 17% -3dB $|S_{21}|$ bandwidth and 1.5dB insertion loss is demonstrated. The footprint size of the filter is $\sim\lambda_0/16\times\lambda_0/9$ @ 2GHz and is 45% smaller than its traditional counterpart.

CHAPTER 1: INTRODUCTION

1.1. Overview

The continuous growth of wireless communication technology demands compact, light-weight, wide-band, multifunctional and efficient antennas and RF circuits. In the past, several miniaturization techniques have been implemented to meet this need but the resulting antennas suffer from fundamental limitations [1]. As described in [1], the maximum gain-bandwidth product of a resonant antenna sets a fundamental constraint on the physical size of the antenna. Thus, designing an antenna with reasonably high gain with required bandwidth and compact physical size proves to be a major challenge to an antenna engineer. Evidently, depending upon the application need, a trade off must be made between the gain and bandwidth once a small antenna with specified dimensions has been designed.

1.2. Antenna Miniaturization Techniques: Background Review

Till date several miniaturization techniques have been implemented in order to obtain electrically small antennas. These techniques can be broadly classified into three categories: changing substrate parameters, modifying the radiator geometry and altering the geometry of the ground plane. A review of these miniaturization techniques along with the issues related with it are discussed below.

1.2.1 Modifying Substrate Parameters

Literature provides various techniques by which substrate parameters and electromagnetic fields confined within the antenna body can be changed. One of the most

common techniques is to use shorting plates [2] or shorting pins [3, 4] which shifts the voltage null away from the center of the radiating element. The level of miniaturization achieved with this technique depends on the placement position of the shorting element. By placing the shorting element at the edge of the radiator, a maximum shift of the voltage null can be achieved and the transverse dimension of the antenna can be reduced by 60% [5]. Also, this technique results in low radiation efficiency and narrow bandwidth. Miniaturization by employing high permittivity [6, 7] and permeability [8] materials as the antenna substrates are known to be effective but possess issues associated with machinability and cost of high contrast ceramic substrates [9, 10]. For example, a stacked patch antenna implemented in low temperature cofired ceramic technology (LTCC) has achieved a compact size on a high permittivity (ε_r=14) $\lambda_0/6.8\times\lambda_0/6.8$ LTCC tape [11]. Reference [9] carried out the stacked patch design over a higher permittivity (ε_r=45) ceramic substrate and realized an overall antenna size of $\sim\lambda_0/8\times\lambda_0/8$ around the L2 (1227MHz) band. Recently, design flexibilities offered by the metamaterial inspired antennas [5, 12-16] have been harnessed to develop small antenna elements. Although, all these techniques provide a considerable amount of miniaturization, however, impedance matching, small bandwidth, low radiation efficiency, increased fabrication complexities and cost of high contrast ceramic substrates still remains the design challenges. Alternative designs based on printed metamaterials [17] were considered to reduce the antenna footprint for low-profile monopoles [18] and patches [19]. Nevertheless, low radiation efficiency and narrow bandwidth continue to be a challenge. Recently, several research groups have adopted engineered negative permeability (i.e. MNG) substrates made-up from periodic arrangements of spilt ring resonators (SRRs) as an alternative miniaturization technique [14, 16, 20]. However, the necessary vertical alignment of the SRRs with respect to the antenna ground plane significantly increased the

fabrication complexity and associated cost. More recently, inspired from the fact that periodic arrangements of complementary versions of split ring resonators (CSRRs) can generate an engineered negative permittivity (i.e. ENG) material [21], a new miniaturized patch has been realized by horizontally placing a CSRR between the ground and antenna metallization planes [5]. This antenna has been designed by utilizing a genetic algorithm optimization approach and can only radiate with linear polarization due to its rotationally asymmetric layout.

1.2.2 Modifying Radiator Geometry

The second miniaturization technique involves changing the radiator geometry to 3-D such as folded patch [22], inverted L/U shape patch [23, 24] and, folded cubical dipole [25]. But this hampers the mechanical robustness of the design. Other traditional techniques such as meandering [26, 27] are also employed for antenna miniaturization. Nevertheless, low radiation efficiency and small bandwidth continue to be the major limitation factors. In addition, placing slots on the radiator is also a very common approach [28, 29]. However, the level of miniaturization (typically 38%, [2]) is limited to the extent by which current path is elongated. In [24, 30], fragmented aperture method was employed for miniaturization but the antenna was yet about $\sim\lambda_0/5\times\lambda_0/5$ at the L2 band.

1.2.3 Modifying Ground Plane Geometry

Lastly, etching slots on the ground plane also provides considerable antenna size miniaturization such as in [31-33]. In [34-36] it is reported that by etching arrays of SRRs into the ground plane (creating complementary SRRs or CSRRs) it is possible to lower the resonant frequency of the patch to that of the CSRRs. However, this approach only provides modest size reductions (about 32% reported in [34]). Nevertheless, this results in a significant reduction in front-to-back ratio (to almost 0dB, [5]) and increases the cross polarization level to the same

level as the co-polarization in both E- and H- planes. Moreover, the etched slot pattern consumes more space than the radiating element thereby keeping the overall size of the design unaffected.

It is also important to point out that all these miniaturization techniques mentioned above aim to reduce the antenna metallization footprint without considering the substrate size. That is to say, although the footprint size of the antenna was reduced, its overall size (which includes the substrate size) was kept the same.

1.3. Filter Miniaturization: Background Review

In the past, numerous state-of-art filters have been reported [37-43] to achieve this. These filters are implemented in low temperature co-fired ceramic (LTCC) substrate technology, containing approximately ten layers or more of metallization layers connected through several vias. The proposed designs have good performance and are very compact in size. However, they have complex design structure which leads to complicated synthesis process and high fabrication cost. In [41, 44, 45], size of the filters has been reduced by using quarter-wave transformers. Although, these filters demonstrate good performance, their structures are complicated due to use of folding topology and mass of shorted vias. Filter miniaturization using lumped reactive elements have been used in the past [46-48], however, they have very poor quality factors, high insertion loss and low rejection at RF frequencies.

1.4. Dissertation Organization

The aim of this presented work is to advance the present state of art in miniaturization techniques in antenna and RF devices. This dissertation is organized in 6 chapters, with chapters 1 and 6 corresponding to introduction and future work. Chapter 2 presents a wide-band CDL antenna design operating in ISM band. The design methodology for obtaining printed compact resonators and predicting its resonance through dispersion diagram analysis will be discussed in

detail. Chapter 3 presents a small compact dual-band circularly polarized CDL antenna along with experimental verifications. The design is shown to operate at GPS L2-L1 bands. In chapter 4, a miniaturized circularly polarized patch antenna is presented. The antenna is designed to operate in ISM band. Finally, in chapter 5 a miniaturization technique to obtain small compact RF filters is presented. The technique of reactive volumetric pin loadings, introduced in chapter 3 and 4, is used for miniaturizing the size of the filters.

CHAPTER 2: MINIATURE COUPLED DOUBLE LOOP (CDL) ANTENNA[1]

2.1. Design Methodology

In our antenna design methodology, we treat a printed antenna as a two unit resonators which are cascaded circularly in a periodic fashion, see Fig. 2.1(a). As shown in Fig. 2.1(b), each of these unit cells is composed of a pair of printed transmission lines. The antenna resonates whenever a standing wave is formed by two oppositely propagating voltage waves. This occurs whenever each wave acquires a phase shift of $(\Phi+n2\pi)$ after traversing the whole loop. Evidently, this condition requires that the phase delay of each unit cell should be an integer multiple of π.

The first step in designing the unit cell is to determine its resonance frequency which is done by extracting its dispersion diagram, also called as $K=\omega$ diagram. A typical dispersion diagram of half loop unit cell composed of a regular TL is shown in Fig. 2.1(c). On this diagram, we can see the resonant frequency of the loop corresponds to the integer multiple of π phase delays. Intuitively, to miniaturize an antenna, its resonance frequency must be lowered without changing its physical size. Thus, our miniaturization goal is to shift down the $K=\pi$ points as lower as possible in the frequency axis without increasing the physical size of the unit cell. This can possibly be done by loading the unit cell with lumped inductors and capacitors, see Fig. 2.1(b). Fig. 2.1(d), depicts the dispersion diagram of the unit cell loaded with lumped inductor

[1] G. Mumcu, S. Gupta, K. Sertel, and J. L. Volakis, "Small Wideband Double-Loop Antennas Using Lumped Inductors and Coupling Capacitors," *Antennas and Wireless Propagation Letters, IEEE*, vol. 10, pp. 107-110, 2011. Permission is included in Appendix A.

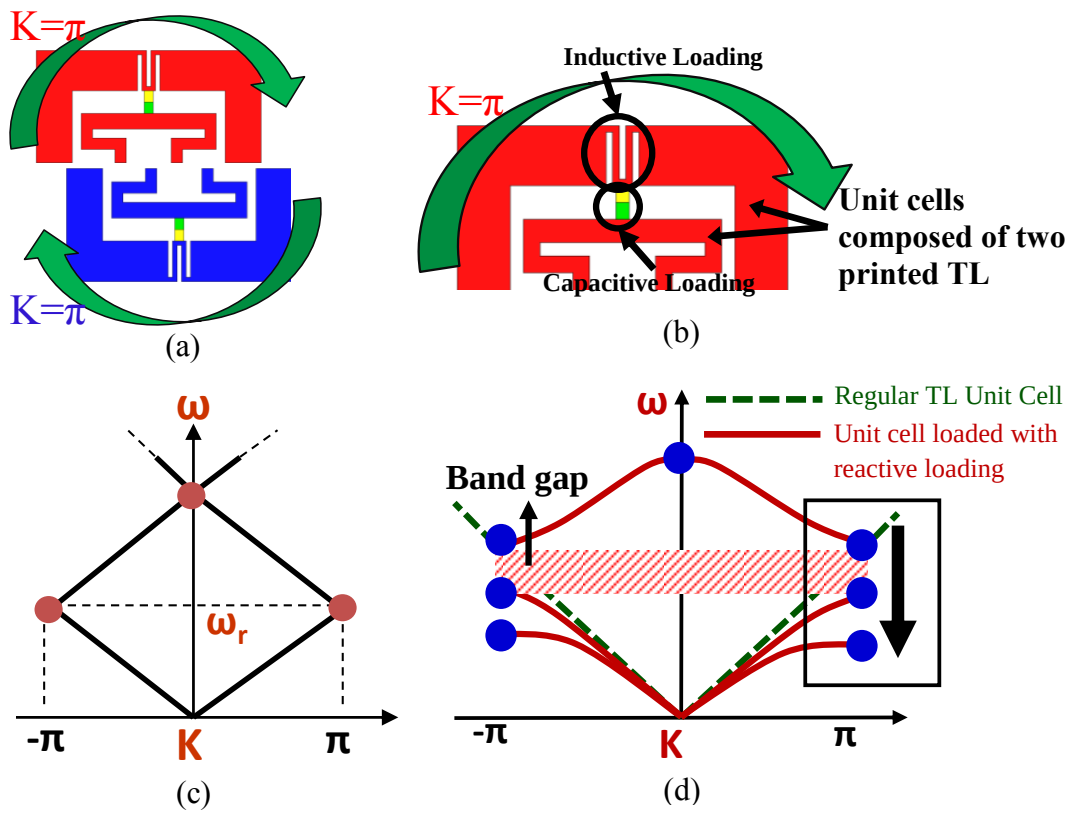

Figure 2.1: CDL antenna layout and dispersion diagram. (a) Two unit cells cascaded circularly; (b) Unit composed of two TL's loaded with reactive loading; (c) Dispersion diagram of a unit cell composed of only a regular TL; (d) K=π resonance shifts down by loading the unit cell with reactive loadings, providing antenna or device miniaturization.

and capacitor (i.e. unit cell of Fig. 2.1(b)). As can be seen, a band gap opens up in the diagram at K=π points. Such a periodic structure is known as a regular band edge (RBE) crystal because of its 2nd order parabolic behavior near the band edge. As shown in Fig. 2.1(d), the resonance at K=π points can be further pushed down to a lower frequency by increasing the loading, thereby providing a 4th order curve. A 4th order curve allows a maximally flat band edge be further pushed down to a lower frequency by increasing the K=π points.

2.2. Dispersion Diagram Analysis Applications

The dispersion diagram and the miniaturization technique discussed above can be applied to obtain small compact radiators. To elaborate it further, two design examples will be discussed

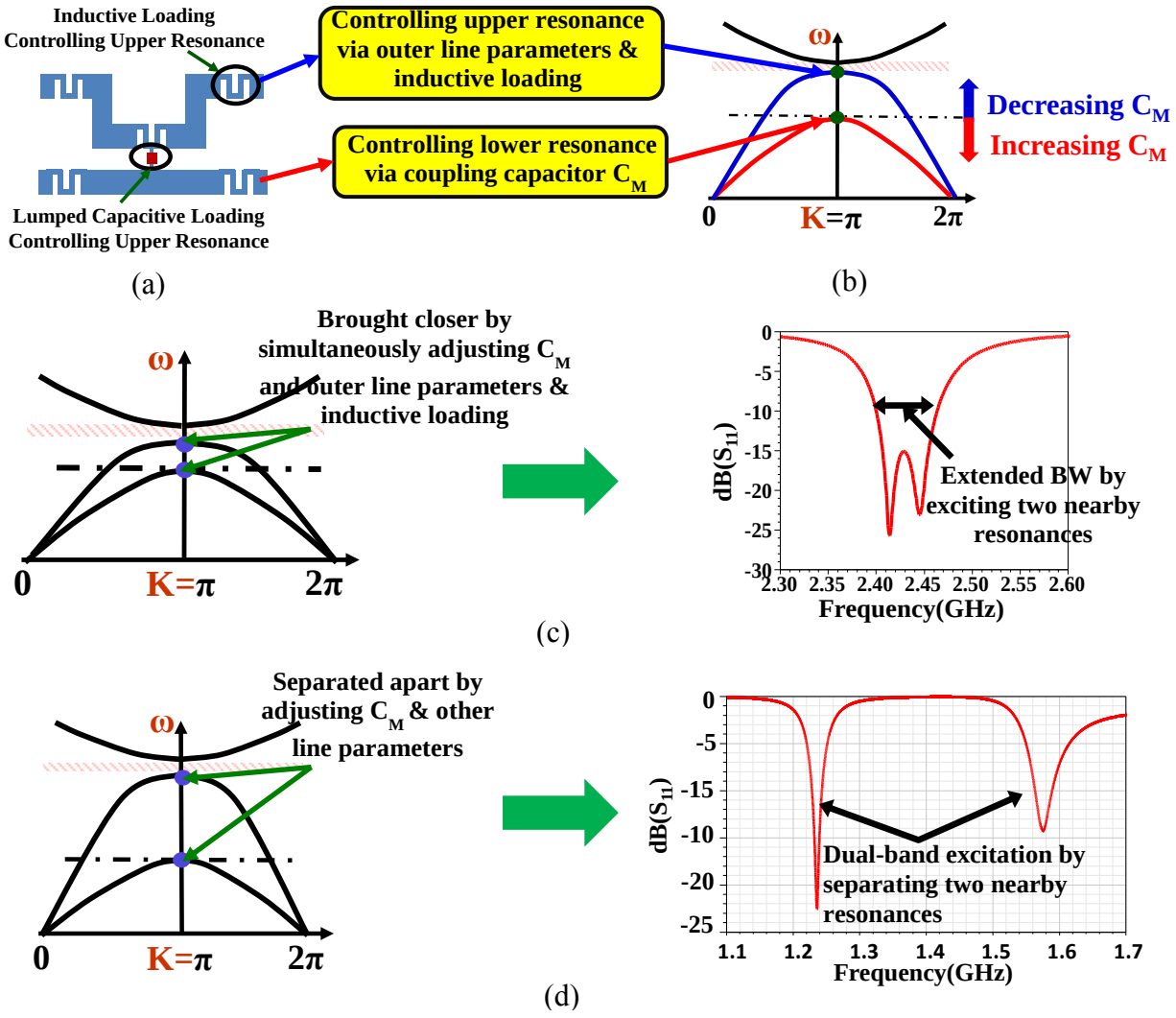

Figure 2.2: CDL unit cell and its applications. (a) Unit cell consisting of partially coupled and reactively loaded microstrip lines; (b) Two unit cells cascaded in a circularly periodic fashion form a resonator operating at K=π frequencies; (c) Bringing two K=π resonances together and simultaneously exciting them results in bandwidth enhancement; (d) Separating the K=π resonances results in dual band performance.

in this and the following chapters.

Fig. 2.2(a), depicts the CDL (coupled double loop) unit cell composed of two partially coupled microstrip lines loaded with lumped circuit loads. Propagation of the waves through this unit cell can be represented with the dispersion (K-ω) diagram shown in Fig. 2.2(b). Due to the presence of multiple microstrip lines, these K-ω diagrams exhibit multiple branches and allow

the antenna to support radiation simultaneously at different bands. In addition, lumped circuit loads (i.e. inductors and coupling capacitor (C_M)) could be strategically employed within the antenna layout to achieve miniaturization without resorting to high contrast (ε_r>10) ceramic substrates. The shape of the dispersion diagram and separation of the K=π frequencies are conveniently controlled with the microstrip line widths, lengths, and lumped circuit loads [49]. Precisely, the upper band resonance can be controlled via outer line parameters (i.e. TL length and width) and lumped inductors whereas, lower band resonance can be controlled by adjusting coupling capacitor (C_M), see Fig. 2.2(b). The design flexibility of adjusting the frequency spacing between the K=π resonances allow us to obtain two different antenna types. For the first case, an extended bandwidth performance can be achieved by bringing closer two consecutive K-ω branches and simultaneously exciting their K=π resonances, see Fig. 2.2(c). In contrast, a dual-band performance can be obtained by tuning the K=π resonances associated with each branch of the K=ω diagram (see Fig. 2.2(d)) to the desired frequencies via proper selection of the unit cell parameters. In the following section CDL wide-band antenna design is discussed. The rest of the chapter 2 discuss about the design procedure to extract the complete antenna layout for CDL wide-band antenna, whereas, its dual-band counterpart will be discussed in detail in chapter 3. To support our study, fabricated prototypes with its measured results are presented.

2.3. Miniature Coupled Double Loop (CDL) Antenna with Extended Bandwidth Performance

As depicted in Fig. 2.3, CDL antenna is formed by cascading two partially coupled microstrip line layouts in a circularly periodic fashion. The antenna resonates at K=π frequencies, since these points are associated with matching phases of the two propagating waves (K>π and K<π). Antenna miniaturization is obtained by lowering the K=π resonances. Concurrently, an extended bandwidth performance can simply be achieved by bringing two

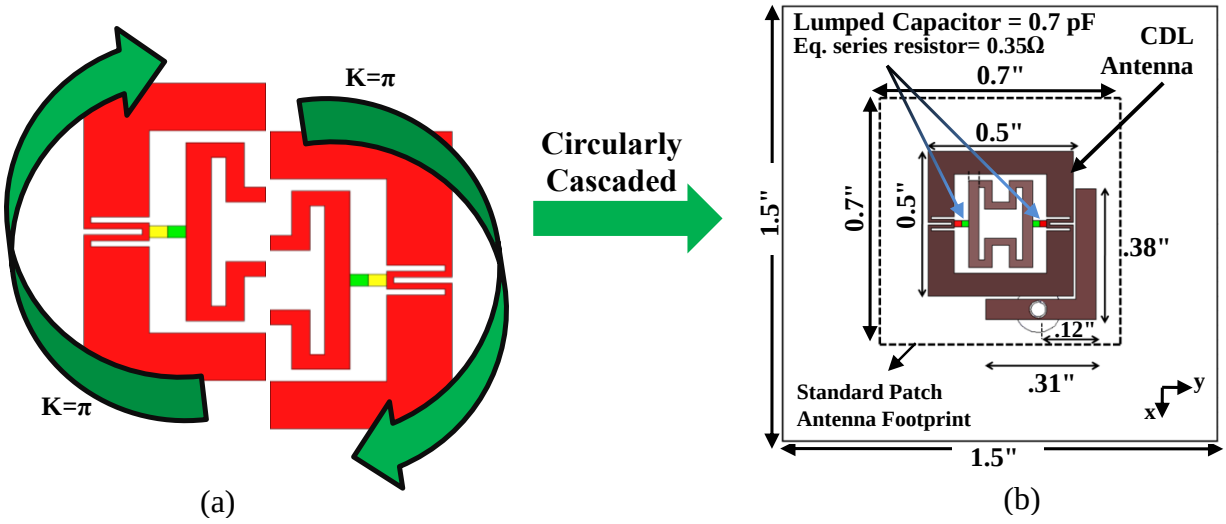

Figure 2.3: Simulation model of CDL wide-band antenna. (a) Circular cascading of two unit cells to obtain a complete resonator with a phase shift of 2π; (b) Capacitively loaded double loop (CDL) antenna layout on 125mil thick 1.5" × 1.5" Rogers TMM 10i (ε_r=9.8, tanδ=0.002) substrate vs. patch antenna footprint.

consecutive K-ω branches close to each other and simultaneously exciting their K=π resonances.

The following sections present three miniature CDL antennas designed via a K-ω diagram analysis that treats the antennas as two unit cell resonators. One of the antenna prototypes is fabricated on a 125-mil-thick Rogers TMM10i substrate and shown to deliver 2.1% $|S_{11}|$ < 10-dB bandwidth and 1.2 dB gain with a $\lambda_0/9.8$ x $\lambda_0/9.8$ x $\lambda_0/39.4$ footprint at 2.4GHz. This CDL antenna has 49% smaller footprint area than a standard patch while achieving a similar bandwidth performance. The second CDL antenna is fabricated on a smaller substrate having comparable size to its footprint. Despite being 45% smaller, this CDL antenna exhibits the same bandwidth performance as the standard patch. The other CDL antenna was shown to exhibit 14.7% bandwidth from 2.4 to 2.78 GHz on a 250-mil-thick substrate. Its footprint is $\lambda_0/9.8$ x $\lambda_0/9.8$ x $\lambda_0/19.7$ with a gain of 4.34 dB (>80% efficiency) at 2.4.

2.4. Antenna Design and Operation Principle

To demonstrate control of the resonance frequency spacing and bandwidth enhancement using coupled microstrip lines, we consider the unit cell layout depicted in Fig. 2.4(a). The unit cell footprint has dimensions of 500 x 250 mil on a 125mil thick (1mil = 0.001 inch = 0.0254mm) substrate. To enable circular cascading [40] (thus, carry out dispersion analysis), the microstrip ports were aligned at y = 0 the cut as depicted in Fig. 2.4(b). A high-contrast substrate with relative permittivity ε_r = 9.8 was used to achieve a smaller footprint. Previous work on lumped circuit unit cell models [41] demonstrated that one of the K = π frequencies can be controlled via coupling and the other K = π frequency is primarily associated with the length and reactive load on the outer line. Therefore, a lumped capacitor C_M was placed between the inner and outer lines [see Fig. 2.4(a)] to achieve greater control and adjust separation of the K = π resonances. A meandered inductor was also introduced to bring the resonance associated with the outer line down to the 2.45 GHz ISM band. We also remark that the line width was shown to be critical for the CDL bandwidth [39], [40]. Specifically, to improve bandwidth, we chose the outer microstrip lines to be ~80mil, which is considerably wider than the inner line width of ~25mil.

Since the substrate thickness is larger than the line widths, and the ports are closely spaced (due to the small footprint size), a full-wave eigenfrequency analysis is needed to extract the K-ω diagram. Fig. 2.4(b) depicts the computational model for eigenfrequency analysis. To model the circular periodicity, two periodic boundary conditions were employed on x > 0 and x < 0 segments of the y = 0 plane. A 5-mil-thick perfect electric conductor (PEC) strip was used to separate these periodic boundary conditions from each other as shown in Fig. 2.4(b). To terminate the computational domain, PEC boundary conditions were placed adjacent to the

substrate walls and 1000 mil above the substrate surface. We also note that losses in conductors, lumped capacitor, and substrate were ignored for carrying out the dispersion diagram analysis. Fig. 2.4(c)–(e) depicts the K-ω diagrams of the unit cell for various C_M values. As seen in the unloaded (C_M = 0pF) case (see Fig. 2.4(c)), two K = π resonances are observed at 2.86 and 2.46 GHz. As expected from the lumped circuit models [41], C_M increases coupling and modifies the shape of the K-ω branches (lowers one of the K = π resonances). For this unit cell configuration, the frequency of the lower K = π resonance is primarily controlled by the outer line length. In our design, the lumped meandered inductor was first chosen so that a K = π resonance was obtained

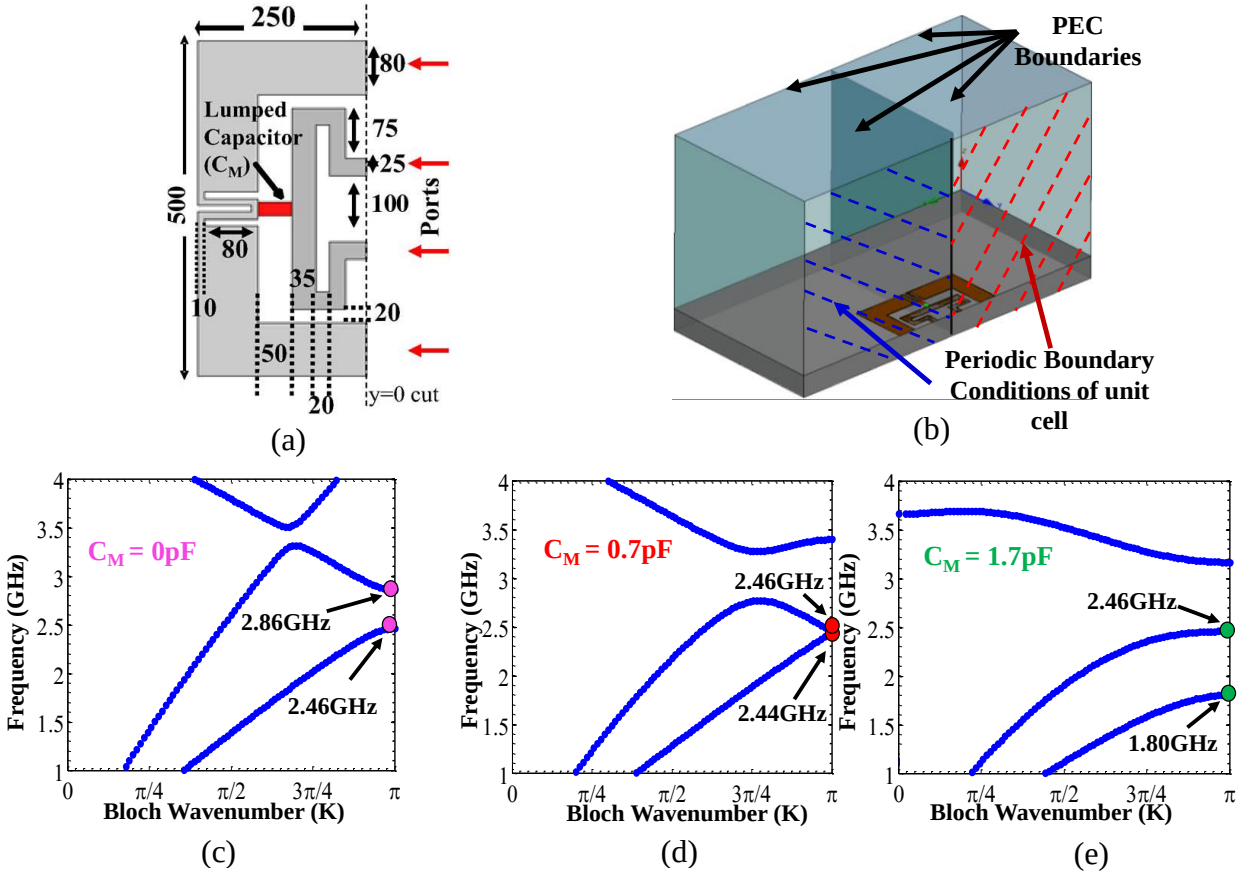

Figure 2.4**:** Unit cell layout and computational model for dispersion diagram analysis. (a) Unit cell layout (dimensions are in mils); (b) Computational model for eigenfrequency analysis. Dispersion diagram for (c) C_M = 0pF, (d) C_M = 0.7pF, and (e) C_M = 1.7pF. Proper C_M loading can tune one of the K = π frequencies.

at 2.46 GHz. Subsequently, C_M was increased to bring the second K = π resonance in proximity to the first. As depicted in Fig. 2.4(d), for C_M = 0.7pF, the K-ω branches exhibit K = π resonances at 2.46 and 2.44 GHz, forming the two closely spaced resonances about the center frequency of 2.45 GHz. Fig. 2.4(e) shows the C_M = 1.7pF case, resulting in two well-separated resonances at 1.8GHz and 2.46 GHz. To summarize, the presented unit cell can exhibit dual resonances controllable via C_M and meandered inductor values. In the following, we present the realization of specific antenna designs that achieve extended bandwidth performance based on this concept.

2.5. Antenna Performance

CDL antenna was formed by cascading two partially coupled microstrip line unit cells in a circularly periodic fashion as depicted in Fig. 2.5(b). A fabricated prototype of the CDL antenna is shown in Fig. 2.5(a). This antenna was implemented on a 125-mil-thick 1.5 x 1.5 in Rogers TMM10i (ε_r = 9.8, tanδ = 0.002) substrate. Its footprint was etched from copper and, as usual, the substrate's back surface was metallized to form the ground plane. For performance comparison, a standard patch antenna with a footprint of 0.7 x 0.7 in^2 was also fabricated to match the CDL antenna's resonance, as depicted in Fig. 2.5(a).

The CDL antenna in Fig. 2.5(b) was fed by a capacitively coupled 50- coaxial probe and a microstrip feed line. The lengths of the feed line along the x- and y-axes were adjusted to achieve matching at the higher and lower resonance frequencies, respectively. For C_M = 0.7pF coupling, the calculated resonances at 2.41 and 2.44 GHz [see Fig. 2.5(b)] result in an extended bandwidth of 2.5%. These resonances deviate slightly from the corresponding 2.44 and 2.46 GHz values obtained via dispersion analysis. Such deviations between the K-ω diagram resonances and the actual ones are expected [40]. It is due to the feed structure that perturbs the

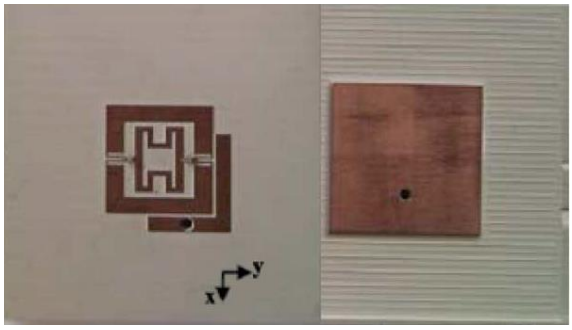

(a)

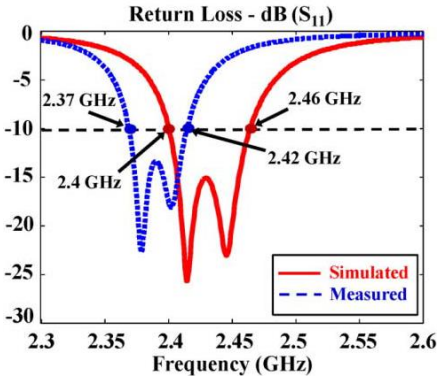

(b)

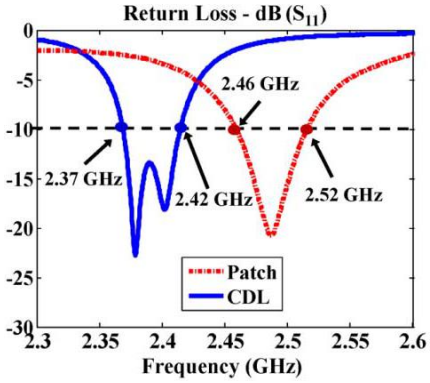

(c)

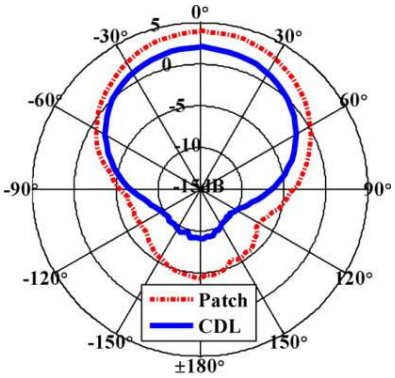

(d)

Figure 2.5: Fabricated antenna prototype and its performance. (a) CDL and patch antennas fabricated on a 125-mil-thick Rogers TMM10i substrate. Both antennas operate near the 2.45 GHz ISM band; (b) Comparison of simulated and measured return loss for the CDL antenna; (c) Measured return loss of the CDL and patch antennas; (d) Measured x-directed polarization gains (patch at 2.49 GHz, CDL at 2.4 GHz) in the y-z plane.

periodicity and the computational model approximating the domain truncation with PEC walls. Nevertheless, the dispersion analysis serves well for design guidance.

To improve impedance matching at 2.4 GHz, the feed line oriented along the x-axis was further extended by 20mil using copper tape. From Fig. 2.5(b), we observe that the measured bandwidth curve is in reasonable agreement with the simulated one. Specifically, a 2.1% bandwidth from 2.37 to 2.42GHz was measured for the CDL antenna. Fig. 2.5(c) and (d) presents the measured bandwidth and gain performances of the fabricated CDL and patch antennas. It is seen that the CDL antenna has similar bandwidth performance to the patch (2.1%

versus 2.3%) while being 49% smaller in footprint area. The measured x-directed polarization gains for the CDL antenna were 2.2 dB at 2.40 GHz and 1.2 dB at 2.38 GHz. The corresponding patch antenna gain was measured to be 4 dB at 2.49 GHz. That is, the CDL antenna can deliver the same bandwidth with a significantly smaller footprint area at the expense of reduced gain (~2 dB less gain) and radiation efficiency (~65%). Regardless, it is important to note that the CDL antenna footprint was only $\lambda_0/9.8 \times \lambda_0/9.8 \times \lambda_0/39.4$ at 2.4GHz

2.6. Substrate Size Effects

The small footprint of the CDL antenna implies that the substrate size could also be reduced significantly. To better assess the CDL antenna's performance on a small substrate, the substrate size was reduced down to 0.6 x 0.6in^2. Thus, as depicted in Fig. 2.6(a), the antenna could barely fit on the substrate. The antenna was fed with a capacitively coupled 50Ω coaxial probe, and its design was carried with the antenna centered on a 1.5 x 1.5in^2 brass ground plane. As depicted in Fig. 2.6(b), the CDL antenna exhibited two closely spaced resonances about 2.54 GHz and had a bandwidth of 1.6%. The increase in the resonance frequencies (from the previous design operating at 2.4 GHz band) is attributed to the reduced substrate size. When compared to a reduced size patch [see Fig. 2.6(a)] resonating at the same frequency, the CDL antenna is 44% smaller with its bandwidth still being the same. However, the measured gain given in Fig. 2.6(c) is 2.1 dB at 2.4 GHz and 2.3 dB lower than that of the patch, implying 53% radiation efficiency.

The bandwidth and radiation efficiency of the CDL antennas can be increased significantly by employing a thicker substrate [40]. To verify this, a third CDL antenna was designed using a 250mil thick 1.5 x 1.5in^2 Rogers TMM10i substrate, as shown in Fig. 2.7(a). Similarly to the previous designs, this antenna was configured to have a 500 x 500 mil^2 footprint (i.e. $\lambda_0/9.8 \times \lambda_0/9.8$ at 2.4 GHz) and excite two nearby resonances. Since the $K = \pi$ resonance

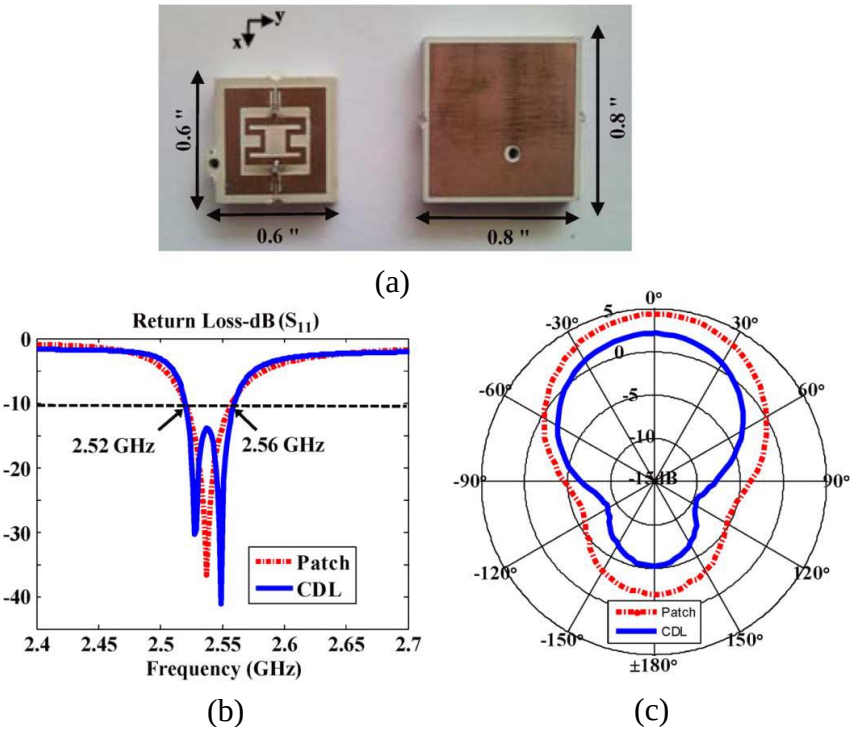

Figure 2.6: Performance comparison of the CDL and patch antennas with reduced size. The measurements are carried out on a 1.5 x 1.5in^2 ground plane. (a) Fabricated antennas; (b) Measured return loss of the CDL and patch antennas; (c) Measured x -directed polarization gains in the y-z plane at 2.54 GHz.

associated with the outer loop is already at about 2.4 GHz (due to the increased fringing fields within the thicker substrate), the meandered inductors were not needed. Also, the outer microstrip lines along the y- axis were chosen somewhat narrower (80 mil) as compared to the 120mil wide lines along the -axis. This was motivated from [40] because such configurations exhibit larger bandwidths at the expense of a larger footprint. This antenna was again fed by a capacitively coupled coaxial probe. The probe was placed on the outer loop, and its location (170mils from the right edge) was adjusted for impedance matching. To further improve matching (during the experiment), a lumped capacitor was connected between the probe and the outer transmission line as shown in Fig. 2.7(a). The value of this capacitor (0.4 pF) was determined experimentally via trial and error. From Fig. 2.7(b) and (c), we observe that the

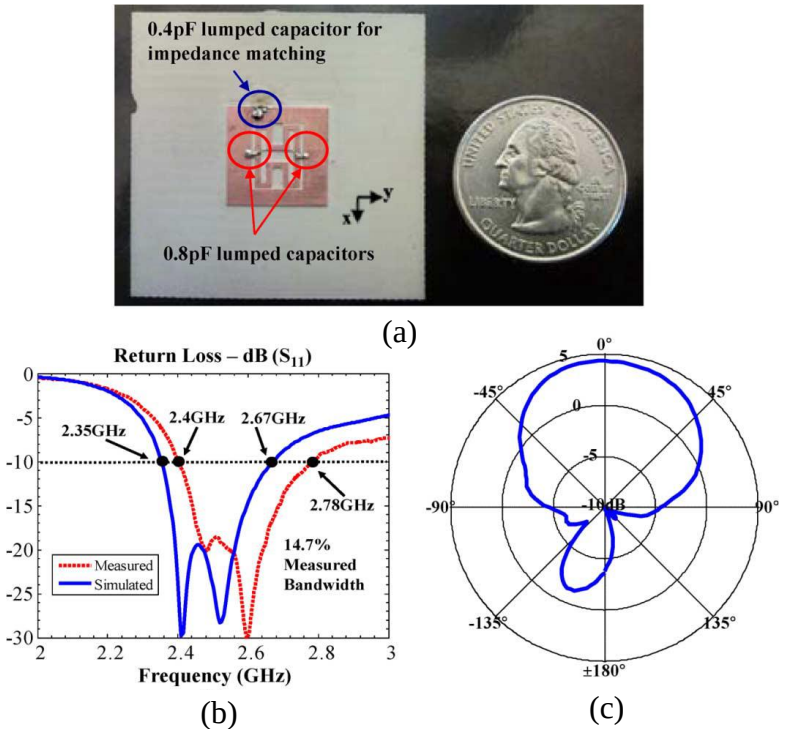

Figure 2.7: CDL wide-band antenna on thicker substrate. (a) CDL antenna fabricated on a 250-mil-thick Rogers TMM10i substrate, An additional lumped 0.4pF capacitor is connected between the coaxial probe and outer microstrip line to improve S_{11} < -10 dB matching. (b) Comparison of simulated and measured return loss. (c) Gain pattern measured at 2.65 GHz in the y-z plane.

measured gain and bandwidth curves are in reasonable agreement with the simulated ones. Specifically, 14.7% bandwidth from 2.4 to 2.78GHz was measured. This CDL antenna exhibited 4.34dB gain at 2.65GHz for the x-directed polarization. The maximum cross-polarization gain level was determined to be 6.5 dB lower than the co-polarization gain across the entire bandwidth. The cross-polarization levels can be further reduced by employing better feeding mechanisms and by resorting to more symmetric unit cell layouts. The radiation efficiency was found to be above 80% over the entire bandwidth (via a gain comparison method). It is important to note that antenna footprint was only $\lambda_0/9.8 \times \lambda_0/9.8 \times \lambda_0/19.7$ at 2.4 GHz.

Based upon our discussion, it can be concluded that an extended bandwidth performance can be obtained by combining two closely spaced K=π resonances via simultaneously adjusting

the unit cell parameters. In contrast, instead of combining the two K=π resonances, a dual band performance can be achieved by separating them apart and precisely tuning them to the desired frequency bands (GPS L2 (1227.5MHz) and L1 (1575MHz) bands for the present case) by controlling the unit cell parameters, as will be discussed in the following chapter.

CHAPTER 3: DUAL-BAND MINIATURE COUPLED DOUBLE LOOP GPS ANTENNA LOADED WITH LUMPED CAPACITORS AND INDUCTIVE PINS[2]

3.1. Introduction

Relatively weak signal level of the Global Positioning System (GPS) makes it inherently vulnerable to intentional or unintentional jammers [50]. Military systems generally address this drawback by employing multi-element GPS arrays to generate pattern nulls in the directions of the jamming signals [51]. Integration of such anti-jam GPS arrays with compact unmanned vehicles and portable devices demands efficient miniature multi-band antenna elements.

To address the above need, several techniques [52-54] have been applied in literature for

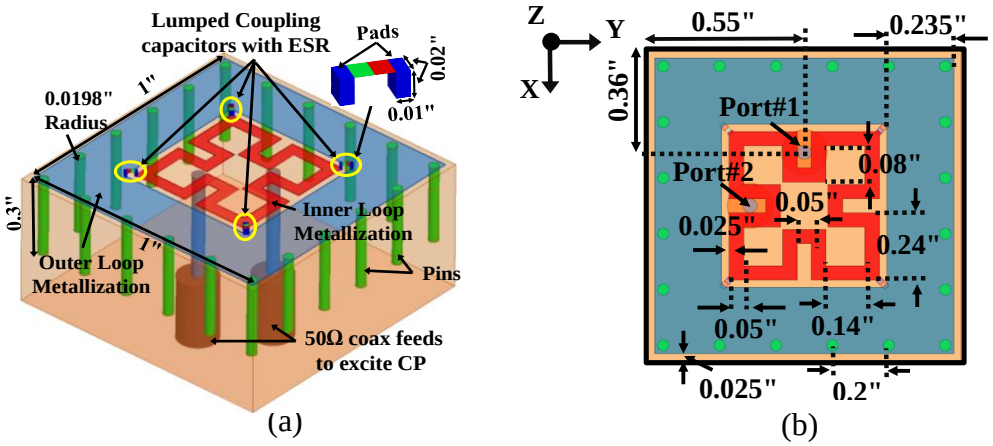

Figure 3.1: Computational model of the dual band CDL GPS antenna. The 0.3" long conductive pins are electrically connected to the outer loop metallization: (a) Lateral view; (b) Top view with detailed layout dimensions.

[2] S. Gupta and G. Mumcu, "Dual-Band Miniature Coupled Double Loop GPS Antenna Loaded With Lumped Capacitors and Inductive Pins," *Antennas and Propagation, IEEE Transactions on*, vol. 61, pp. 2904-2910, 2013. Permission is included in Appendix B.

miniaturization of dual-band GPS antennas operating at the L2 (i.e. 1227MHz) and L1 (i.e. 1575MHz) frequencies. For example, a stacked patch antenna implemented in low temperature cofired ceramic technology (LTCC) has achieved a compact size over a high permittivity (ε_r=14) λ_0/6.8×λ_0/6.8 LTCC tape [11]. Reference [9] carried out the stacked patch design over a higher permittivity (ε_r=45) ceramic substrate and realized an overall antenna size of ~λ_0/8×λ_0/8 around the L2 band. Although this antenna is miniaturized, impedance matching and fabrication of such elements are possibly challenging due to the issues associated with machinability and cost of high contrast ceramic substrates [10, 55]. In [30], fragmented aperture method was employed but the antenna was yet about ~λ_0/5×λ_0/5 at the L2 band. In addition, [56] used quadruple inverted-F with a multilayered feed structure to achieve a compact circularly polarized (CP) antenna. Recently, design flexibilities offered by the metamaterial inspired antennas [12] have been harnessed to develop small dual band GPS elements without necessitating the use of high permittivity substrates [13]. These antennas have been shown to operate with λ_0/6.7×λ_0/6.7 area and λ_0/13 antenna height at L2 band. Other traditional antenna miniaturization techniques such as shorting pins and meandering [26] were also employed for GPS antenna miniaturization. Nevertheless, low radiation efficiency and small bandwidth continue to be the major limitation factors.

More recently, our group has presented [57] a capacitively loaded coupled double loop (CDL) GPS antenna realized over a standard printed circuit board substrate (Rogers TMM10i (ε_r=9.8, tanδ=0.002)) [58]. However, the antenna suffered significantly from low L2 band radiation efficiencies once its substrate size was reduced below 1.6"×1.6" (1mil=0.0254mm=0.001"). In this work, we present a modified dual-band CDL antenna that can concurrently address operational goals of (i) small form factor, (ii) >24MHz 3dB realized gain

bandwidth at L2/L1 bands, and (iii) >70% radiation efficiency at the L2/L1 band center frequencies. Specifically, the CDL antenna layout is modified to be loaded with lumped capacitors and inductive pins (see Fig. 1) to achieve size miniaturization ($\lambda_0/8.8\times\lambda_0/8.8$ at L2 band), high radiation efficiency (>75%), and proper L2/L1 resonance frequency spacing.

Antenna miniaturization through periodic via and/or lumped capacitor loadings has been recently proposed for various structures. For instance, [18] used inductive vias and lumped capacitors within the context of negative refractive index(NRI) metamaterials to realize a small folded monopole antenna. In [59], two NRI metamaterial based small monopoles were designed to resonate at closely spaced frequencies and subsequently combined to form a compact antenna operating with an extended bandwidth performance. Likewise, [60] used a combination of inductive vias and capacitive loadings to introduce infinite wavelength resonant antennas with monopole like radiation patterns. Additionally, in [61] small slot loops and patches were presented using an artificial transmission line structure that included periodically loaded lumped capacitors. Further, in [62], an irregular ground plane structure composed of conductive vias was employed to parasitically load a patch antenna, and thus achieve a circularly polarized radiator.

This presented work investigates the effects of volumetric pin and lumped capacitor loadings, but in contrast to the aforementioned designs, it does not rely on NRI metamaterials or ground plane perturbation. Instead, a miniature double loop antenna is presented radiating based on the $K=\pi$ resonance mechanism. Although the NRI metamaterial antennas can also exhibit multiple resonances and be designed to radiate at $K=\pi$ resonances, the novelty of the presented antenna lies with the use of coupled transmission line loops to achieve the dual-band operation. In addition, the proposed antenna's compact size and dual–band circular polarization distinguish it from previous CDL designs. The design principles of the proposed antenna are characterized

computationally and validated experimentally. In the following, we begin our discussion by briefly summarizing the performance of the 1.6"×1.6" dual band CDL GPS antenna that was designed in our previous work [57]. Specifically, we emphasize that the L2 band efficiency of this antenna degrades significantly from 75% to 13% as its substrate size is gradually reduced down to 1.1"×1.1". In order to alleviate this issue, in Section 3.3, we introduce volumetric inductive pin loading on the outer loop of the 1.1"×1.1" CDL GPS antenna to remove the excessive conductor loss of the L2 band resonance. Section 3.4 presents a 1.1"×1.1" ($\sim\lambda_0/8.8\times\lambda_0/8.8$ at L2) reactively loaded dual-band CDL antenna operating with 4.9 and 2.6dB realized right handed circularly polarized (RHCP) gains at L2 and L1 bands, respectively.

3.2. Dual-Band CDL GPS Antenna

Fig. 3.2 depicts the layout of the CDL GPS antenna realized in our recent work [57] by making use of the mode diversity observed in partially coupled transmission lines [63]. In this design approach, the antenna metallization is treated as a circularly periodic structure consisting of two unit cells (see Fig. 2(a)). As compared to the unit cells in [58] and [64], [57] redesigned the unit cell to realize a CDL antenna layout with 90^0 rotational symmetry in order to support the circularly polarized radiation. The resonances of the antenna leading to broadside radiation are associated with the $K=\pi$ frequencies of the dispersion diagram that depicts the phase shift per unit cell attained by a propagating wave [64]. As shown in Fig. 3.2(c), the presence of dual transmission lines within the unit cells allow the antenna to support radiation simultaneously at two different frequencies. Unit cell parameters such as width of the microstrip lines, their lengths, lumped reactive loads and coupling capacitors (C_M) can be utilized to concurrently adjust the separation between the $K=\pi$ frequencies and achieve miniaturization without necessitating the use of ceramic substrates exhibiting higher permittivity values (i.e. $\varepsilon_r>10$).

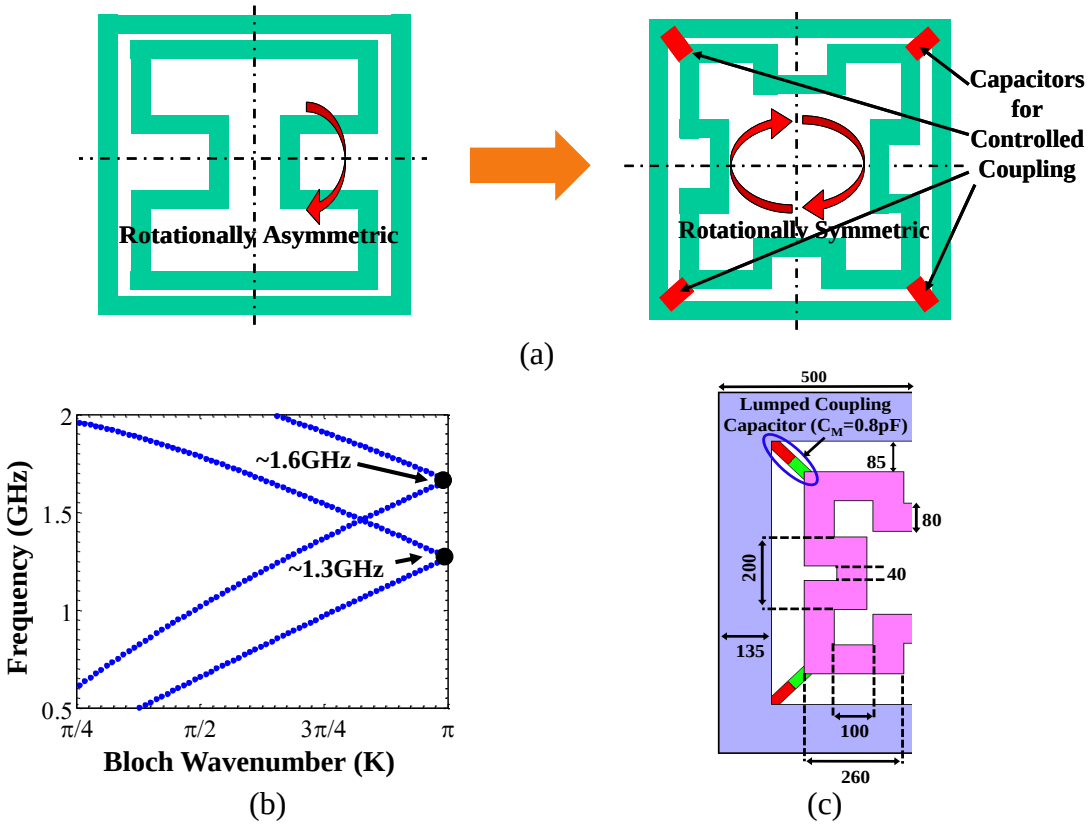

Figure 3.2: Dual-band CDL layout. (a) CDL antenna layout modified to be rotationally symmetric to achieve circular polarization; (b) Dispersion diagram of the unit cell. Two K=π resonances separated to L2 & L1 bands; (c) Unit cell layout (in mils) over the 2"×2" Rogers TMM 10i substrate.

Specifically, the meandered inner transmission line loaded with lumped capacitors is primarily responsible for the 1.6GHz K=π resonance, whereas the 1.3GHz K=π resonance is mainly controlled with the width and length of the outer transmission line. For example, the frequency of the 1.3GHz K=π resonance can be reduced without affecting the frequency of the 1.6GHz K=π resonance if a smaller outer line width is utilized. Likewise, increasing the length of the inner line results in a lower frequency for the 1.6GHz K=π resonance without affecting the 1.3GHz K=π resonance. The increase in C_M results in a lower frequency for both resonances, however, its effect is more pronounced for the higher K=π resonance. Consequently, the CDL antenna accomplishes miniaturization by employing reactive loadings within its unit cell layout

in the form of meandered lines and lumped circuit elements [58]. The metallization area of the unit cell in Fig. 3.2(c) was constrained by 1"×0.5" in the design stage to limit the L2 band electrical size of the antenna metallization by $\sim\lambda_0/10\times\lambda_0/10$. In addition, Rogers TMM10i (ε_r=9.8, tanδ=0.002) was selected as the antenna substrate with 500mil thickness to realize an efficient GPS antenna with satisfactory bandwidth performance. RHCP was achieved by employing two 90º out-of-phase 50Ω coaxial probes within the rotationally symmetric antenna layout. Specifically, the CDL GPS antenna operated over a 10"×10" ground plane with measured 3.4dB (86% efficiency) and 4.4dB (95% efficiency) right handed circularly polarized (RHCP) realized gains at the L2 and L1 bands, respectively.

Our computational studies in [57] identified a significant degradation in the L2 band radiation efficiency as the lateral substrate size of the CDL GPS antenna was gradually reduced from 2"×2" down to 1"×1" (throughout the paper, Ansoft HFSS was used as the design tool). Specifically, a steep drop in L2 band radiation efficiency (12.5% per $0.1"^2$ substrate size reductions) was experienced when the substrate was made smaller than 1.6"×1.6". On the other hand, the efficiency of the resonance mode supporting the L1 band radiation was still found to be larger than 90%. Consequently, the smallest CDL GPS antenna design was previously carried out with a 1.6"×1.6" substrate size to accomplish an efficient L2 band operation. This has motivated us to develop an alternative approach in the design of CDL antenna in order to realize a miniaturized dual-band GPS radiator without a degraded L2 band radiation efficiency.

3.3. Loss Mechanism and Volumetric Pin Loading

To understand the loss mechanism of the L2 mode resonance, computational studies were carried out to evaluate the surface current densities. Since L2 mode radiation is primarily

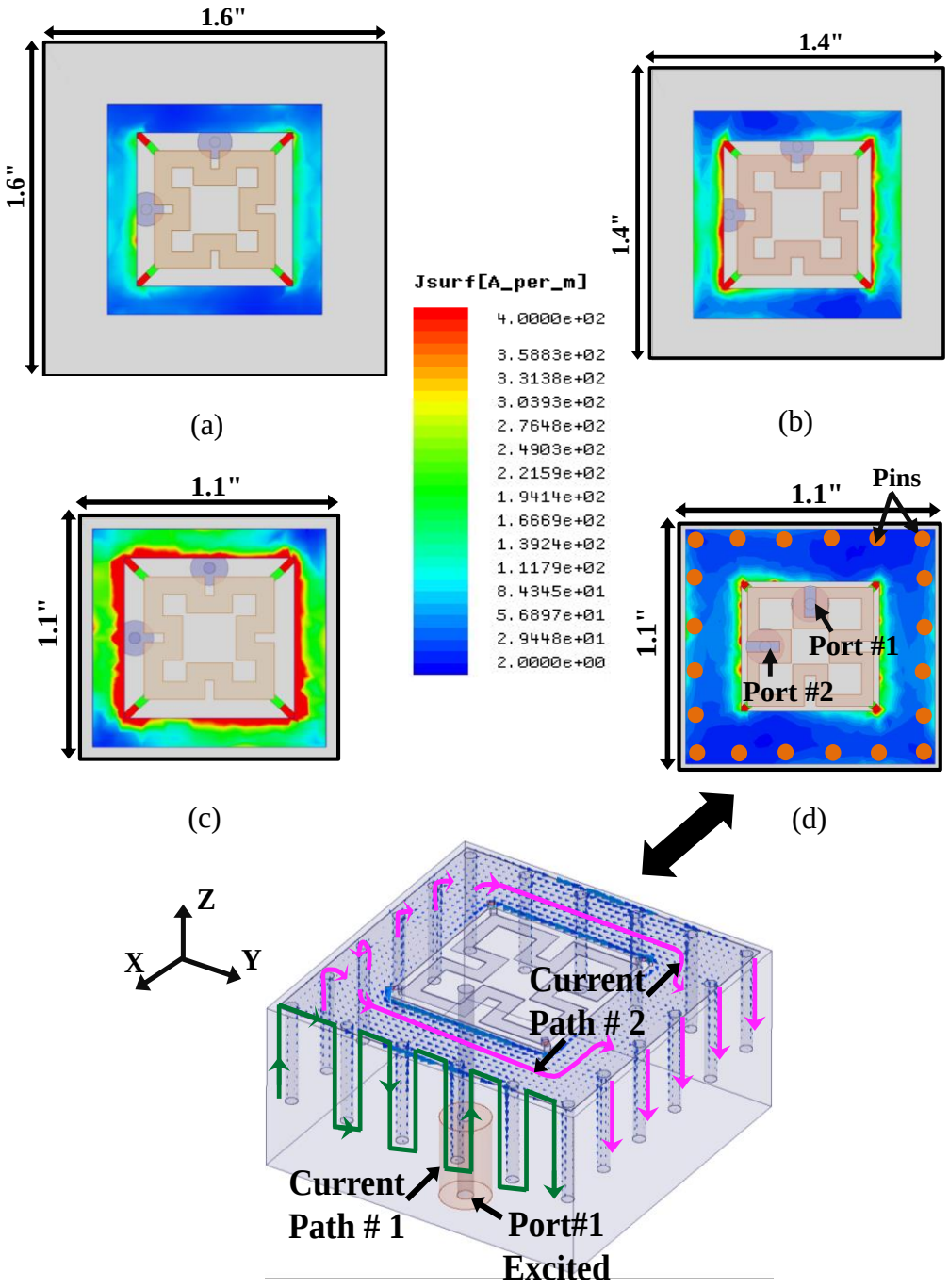

Figure 3.3: Surface current density and current flow. (a) L2 band surface current density on the outer loop with substrate sizes of 1.6"×1.6"; (b) 1.4"×1.4"; and (c) 1.1"×1.1"; (d) 1.1"×1.1" when the outer loop is loaded with 300mil tall 39.6 mil diameter vertical pins; (e) L2 band current flow directions for port 1 excitation.

associated with the outer loop of the antenna layout, Fig. 3.3(a)-(d) present the outer loop's current density for various substrate sizes. From these plots, it is clearly seen that a reduction in substrate size beyond 1.6"×1.6" is accompanied with significant increases in surface current densities at the outer loop and coupling capacitors. Consequently, the conductor losses can be identified as the main cause of the low L2 band radiation efficiency observed in the reduced substrate size CDL GPS antenna.

A well-known approach that can be employed for improving the radiation efficiency of the outer loop is resorting to a wider microstrip line. However, this causes a physically and electrically larger antenna structure. Therefore, we proceeded to decrease the surface current density of the outer loop by distributing the current volumetrically with 0.3" long metalized vertical pins as depicted in Fig. 3.3(d) and (e). These vertical pins were electrically connected to the outer loop metallization and therefore did not make any connection with the ground plane. Fig. 3.3(e) demonstrates the L2 band current distribution on the surface of the pin loaded antenna when the first feed port is excited. It is observed that the currents at the top surface of each unit cell (i.e. half of the antenna) are oriented in the same direction due to the $K=\pi$ resonance, thus, resulting in a broadside radiation. The presence of the pins modifies the current distribution in two different ways. Specifically, the pins on the antenna faces parallel to the x-z plane support a current distribution that serves as an extension length for the surface current on the top of the antenna (see current path #2 in Fig. 3.3(e)). On the other hand, the pins on the antenna faces parallel to the y-z plane provide a reactive loading effect by supporting a meandered current distribution (see current path #1 in Fig. 3.3(e)). Therefore, the loading effect of these vertical pins causes a reduction in L2 band resonance frequency. This effect, in turn, also allows a larger line width for the outer loop without necessitating the enlargement of the antenna size. Since the

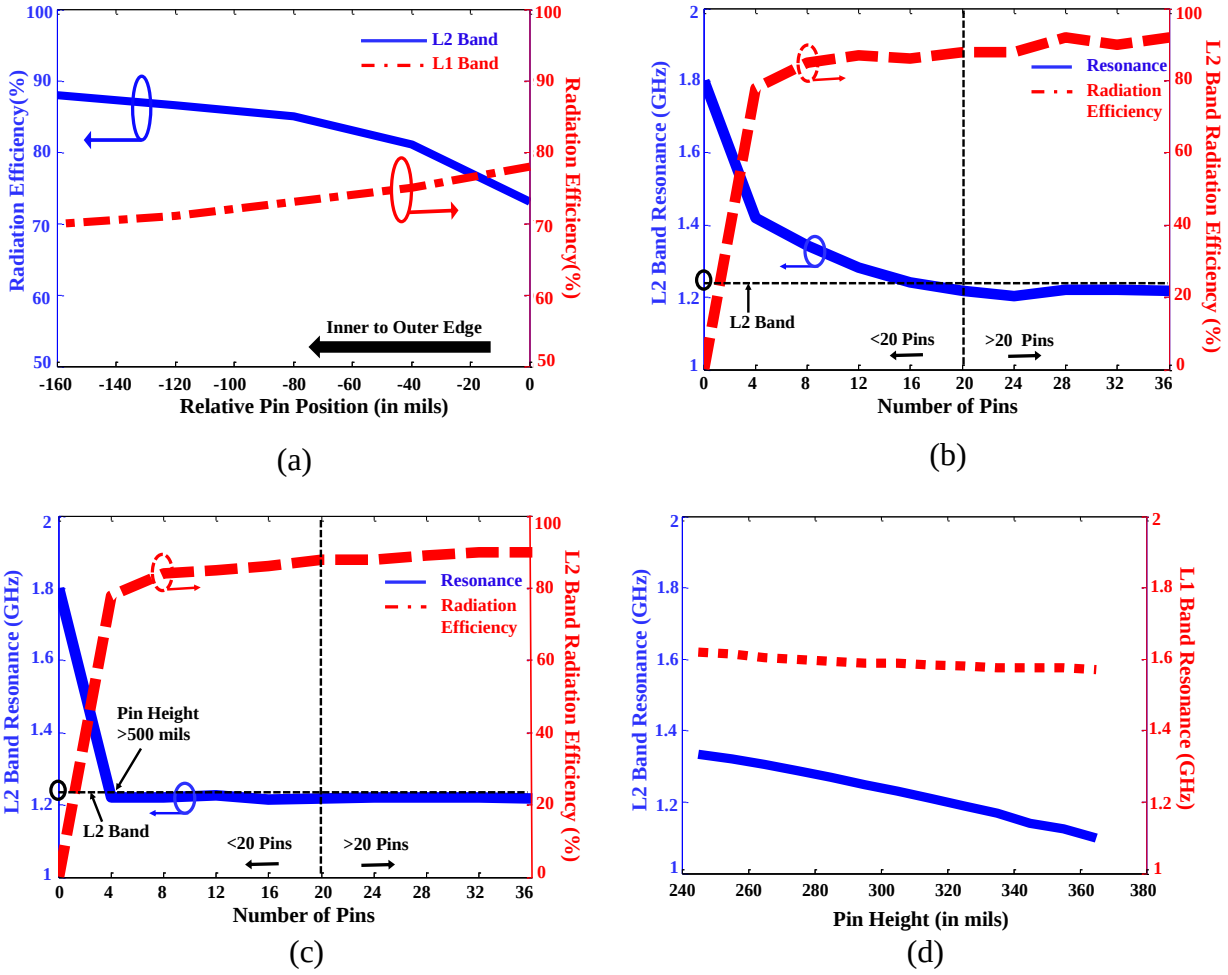

Figure 3.4: Computational study on pin arrangements. (a) Variation in L2 and L1 band radiation efficiencies as the pin locations are changed from inner to the outer edge of the outer loop; (b) L2 band resonance frequency and radiation efficiency as a function of the total number of pins; (c) L2 band radiation efficiency vs. total number of pins as the shift in resonance frequency is compensated by varying the pin heights; (d) Variations in L2 and L1 band resonance frequencies as a function of pin height for the case of N=20.

current is volumetrically distributed, the current densities at the outer loop and capacitors are significantly reduced with the help of these pins. Consequently, the radiation efficiency increases from a mere 13% to 88%. It is also important to note that the presence of the pins at the outer loop does not influence the L1 band surface current density concentrated at the inner loop. Hence, L1 band radiation efficiency is minimally affected with this CDL antenna loading scheme.

To identify the effects of the suggested pin arrangements on the radiation performance, computational studies were carried out to consider various pin parameters such as their relative position along the width of the outer loop, radius, and total number. In these studies, the antenna layout was identical to that of the CDL GPS antenna shown in Fig. 3.1(b). The overall substrate size was 1.1"x1.1" and N=20 300mil long 39.6mil diameter pins metalized from copper were placed at the outer loop. Fig. 3.4(a) presents the variations in the radiation efficiencies of the L2 and L1 band resonances as the pins were gradually re-located from the inner to the outer edge of the outer loop in increments of 20mil. It is observed that the worst-case efficiencies are well above 70% due to the presence of the pins. Specifically, the L1 band radiation efficiency decreases from 78% to 70% as the pins are re- located to the outer edge of the outer loop. On the other hand, the L2 band efficiency increases from 73% to 88% for the same case. Since a standard printed circuit board (PCB) fabrication typically realizes metalized pins from composites having lower conductivities than copper, the outer edge of the outer loop was eventually chosen for the pin locations to maximize the efficiency of the L2 band resonance.

Fig. 3.4(b) depicts the change in the L2 band resonance frequency and efficiency as the total number of the pins are changed from N=0 to N=36. As seen, the antenna is precisely tuned to 1227MHz when the outer loop is loaded with N=20 300mil long pins and radiates with 88% efficiency. When the number of pins are gradually decreased from N=20, the L2 band resonance shifts to higher frequencies, implying an electrically larger antenna structure. On the other hand, increasing the number of pins beyond N=20 does not provide further pronounced benefits in terms of radiation efficiency and electrical size.

Reducing the number of pins without affecting the electrical size, resonance frequency, and radiation efficiency performance is important for achieving a lower cost fabrication. The

resonance frequency shift observed in the L2 band as the number of pins reduced below N=20 can be conveniently compensated by increasing the height of the pins due to elongated current path (see Fig 3.3(e)). As demonstrated in Fig. 3.4(c), longer pins do not significantly degrade the radiation efficiency and the CDL antenna continues to exhibit its miniature size. Nevertheless, the reduction in number of pins is limited by the maximum thickness of the substrate. For example, for N=4, the pin heights must be larger than 500mil to keep the resonance precisely tuned to 1227MHz (i.e. hence, N=4 case was modeled for an antenna residing on 550mil thick substrate). In addition, it may be convenient to restrict the pin height to increments of available substrate thicknesses for a given PCB fabrication approach. For instance, 500mil thick CDL antenna can be realized from a stack of five 100mil thick substrates, thereby allowing a convenient method to realize customized pin heights in increments of 100mil. Consequently, the volumetrically loaded CDL GPS antenna design presented in the following section utilized 300mil long N=20 pins to accomplish the L2 band resonance frequency tuning.

Fig. 3.4(d) demonstrates the sensitivity of the L2 and L1 band resonance frequencies with respect to the pin height (N=20). Specifically, L2 and L1 band resonance frequencies vary by 2MHz/mil and 0.05MHz/mil, respectively. This was utilized in the following section to compensate for the detuning of the fabricated antenna element associated with realization inaccuracies. The computational studies also demonstrated that the L2 band resonance frequency does not significantly get affected by the pin diameters. Therefore, the diameter of the holes to be drilled in the substrate was selected as 39.6mil based on the availability of the drilling tools.

3.4. Volumetrically Loaded Miniaturized CDL GPS Antenna on Reduced Substrate

The computational model of the dual band CDL GPS antenna designed based on the parametric studies of the previous section is depicted in Fig. 3.1. As seen, the overall substrate

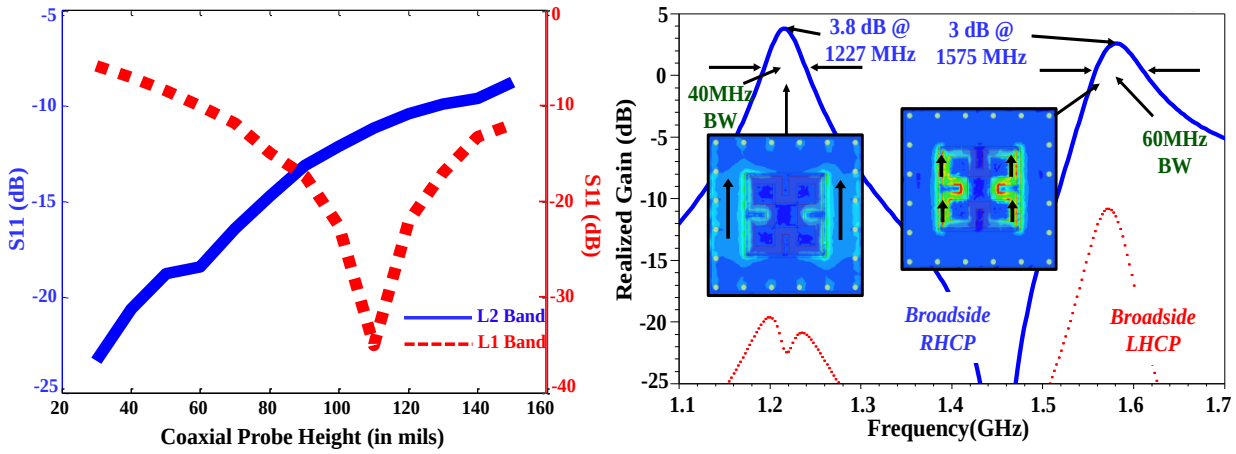

(a) (b)

Figure 3.5: Simulated performance of dual-band CDL antenna. (a) S_{11} performance as the coaxial probe is brought below the top surface of the antenna; (b) Simulated broadside RHCP and LHCP realized gains with current field distributions (for port # 1 excitation) over the top surface of the antenna at L2 and L1 bands. The dominant current flow directions are also indicated with arrows.

size is 1.1"×1.1" and the outer loop is loaded with 300mil long metalized pins. The antenna footprint is 1"×1" and implemented over 500mil thick Rogers TMM10i (ε_r=9.8, tanδ=0.002) substrate. Since the resonant current distribution of the antenna closely resembles that of a printed square loop and meandered square loop antennas at the L2 and L1 bands, respectively (see Fig. 3.5(b)); the bandwidth of the CDL GPS antenna can be modified with the width of the inner and outer loops. In the presented design, 50mil inner and 235mil outer microstrip line widths provided a 3dB realized gain bandwidth >24MHz for both bands. The L1 band resonance frequency was tuned to 1575MHz by utilizing coupling capacitors of C_M=1.2pF modeled with an equivalent series resistance (ESR) of 0.35Ω. To avoid the use of large computational resources, the antenna is modeled to reside over an infinite ground plane and excited by 90^0 offset capacitively coupled coaxial probes. Fig. 3.5(a) demonstrates the L2/L1 band center frequency S_{11} performance of the feed when the coaxial probe is gradually brought down from the top surface of the antenna. Specifically, the probes were selected to be 90mil below the top surface

to provide an equally good impedance match for both of the resonances. The computed $|S_{11}|$<-10dB bandwidths of 10 and 14MHz lead to 3dB RHCP realized gain bandwidths of 40MHz and 60MHz at the L2 and L1 bands, respectively. As shown in Fig. 3.5(b), the antenna operates with peak RHCP realized gains of 3.8dB at the L2 and 3dB at the L1 band, corresponding to 88% and 75% radiation efficiencies respectively. The computed cross-polarization levels are also at least 15dB lower than the corresponding peak gains at the L2 and L1 bands, implying a <1dB axial ratio performance. The current field distributions (for port 1 excitation) plotted over the top surface of the antenna confirms that the L2 band radiation is primarily associated with the outer loop, whereas L1 band radiation is controlled by the inner line parameters and coupling capacitor values.

To verify performance of the design, we proceeded to fabricate a miniature dual-band CDL GPS antenna using four layers of Rogers TMM10i substrates with thicknesses of 250mil, 100mil, 50mil, and 100mil as depicted in Fig. 3.6(a). The initial antenna prototype fabricated using the dimensions of the computational model shown in Fig. 3.1 was observed to exhibit the L2 and L1 band resonances at higher frequencies (i.e. L2 band resonance at 1.4GHz and L1 band resonance at 1.62GHz). This discrepancy between the simulated and measured resonances was found to be primarily associated with the air gaps introduced around the pins. Specifically, in antenna fabrication, cut-wires with 25mil of diameter were used to fill the holes (instead of plating) due to their ease of availability and the observation that the resonance frequencies are not significantly affected by the pin diameters. This manual realization introduced the air gaps around the pins and resulted in a significant resonance frequency deviation. As such, the updated computational model predicted about 0.15GHz resonance shift towards higher frequencies when these air gaps are present. Other potential factors contributing to the difference between the

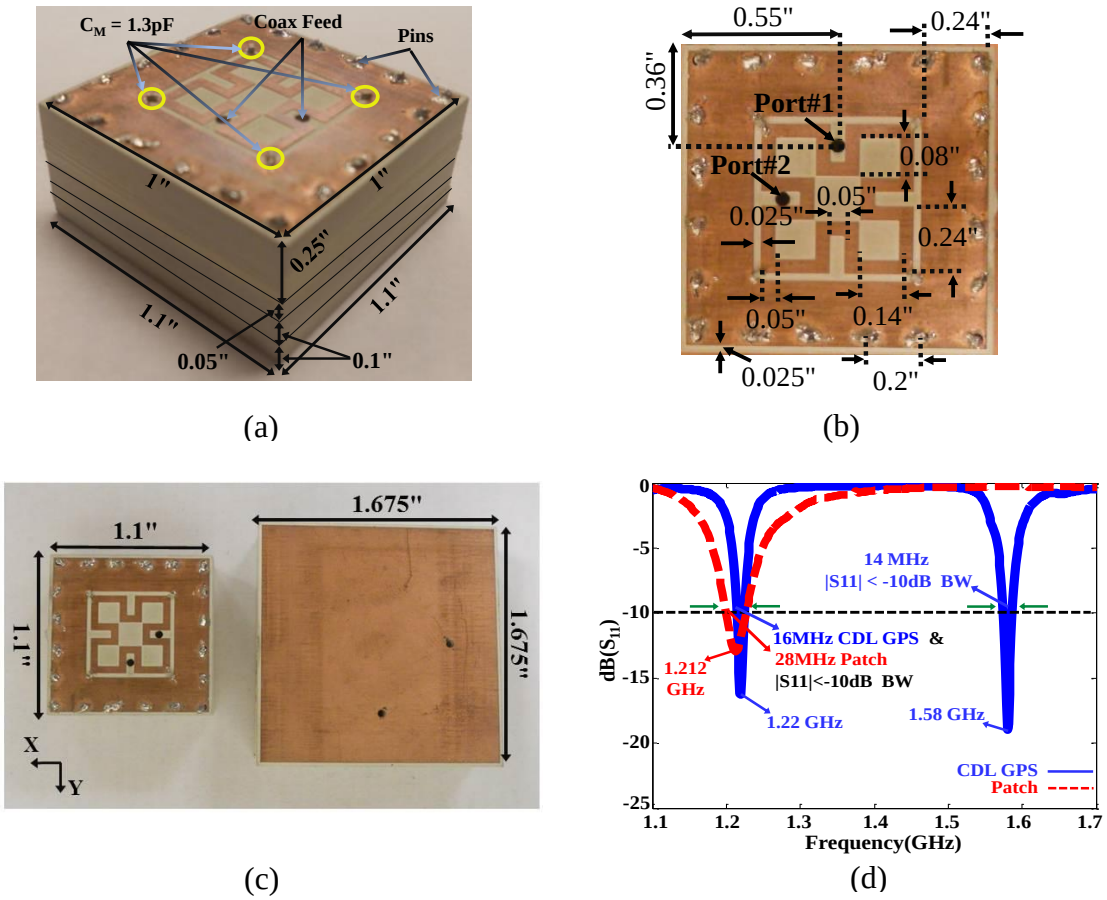

Figure 3.6: Fabricated dual-band CDL GPS antenna on reduced substrate. (a) 3D view; (b) Top view with layout dimensions (pin heights are 400mil); (c) Size comparison between the dual-band CDL GPS antenna and a conventional L2 band patch. Both antennas are designed over the same substrate material and have identical thicknesses; (d) Measured S_{11} performance of the dual-band CDL GPS antenna and the L2 band patch within the 1.1–1.7GHz band.

simulated and measured results are accuracy of the dielectric constant and fabrication tolerances. To tune the resonance frequencies to the close proximity of L2 and L1 frequencies, the antenna prototype was slightly modified. Specifically, the coupling capacitors (obtained from ATC, 0402size) were increased from 1.2pF to 1.3pF to tune the L1 band resonance frequency. Subsequently, pin heights were increased from 300mil to 400mil and a slightly wider outer loop was employed to achieve the L2 band frequency tuning. The 400mil pin heights enabled a convenient realization by making use of the available substrate layer thicknesses. Fig. 3.6(b)

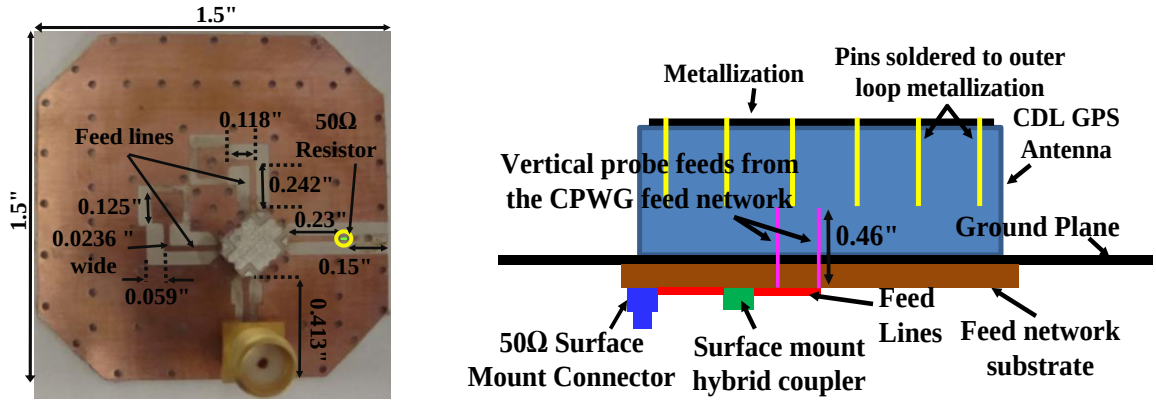

(a) (b)

Figure 3.7: Antenna feed. (a) Fabricated antenna feed structure; (b) Illustration of the feed mounting over the 24"×24"×0.025" brass ground plane.

presents the top view of the dual-band CDL GPS antenna over the 500mil thick 1.1"×1.1" Rogers TMM10i substrate with its finalized footprint dimensions.

To demonstrate the size reduction performance of the miniature dual-band CDL GPS antenna, a standard L2 band patch was also designed and fabricated over the identical 500mil thick substrate material as depicted in Fig. 3.6(c). Fig. 3.6(d) presents a comparison of the S_{11} responses of the miniature CDL GPS and the conventional patch antennas measured over a 24"×24" ground plane using the 50Ω capacitively coupled coaxial probes. Specifically, the CDL GPS antenna resonates at 1220MHz and 1580MHz with $|S_{11}|$<-10dB bandwidths of 16MHz and 14MHz, respectively. On the other hand, the patch provides a much wider bandwidth (28MHz) at the L2 band due to its 60% larger physical size. Nevertheless, as will be shown in the following (see also Fig. 3.8(a)), the 3dB realized gain bandwidth of the CDL GPS antenna still makes it suitable to be employed in the dual-band GPS applications.

The circularly polarized gain of the CDL GPS antenna was measured at the anechoic chamber of the University of South Florida after integrating it with the feed network shown in Fig. 3.7(a). The feed network was implemented over a 25mil thick Rogers 6010.2LM (ε_r=10.2,

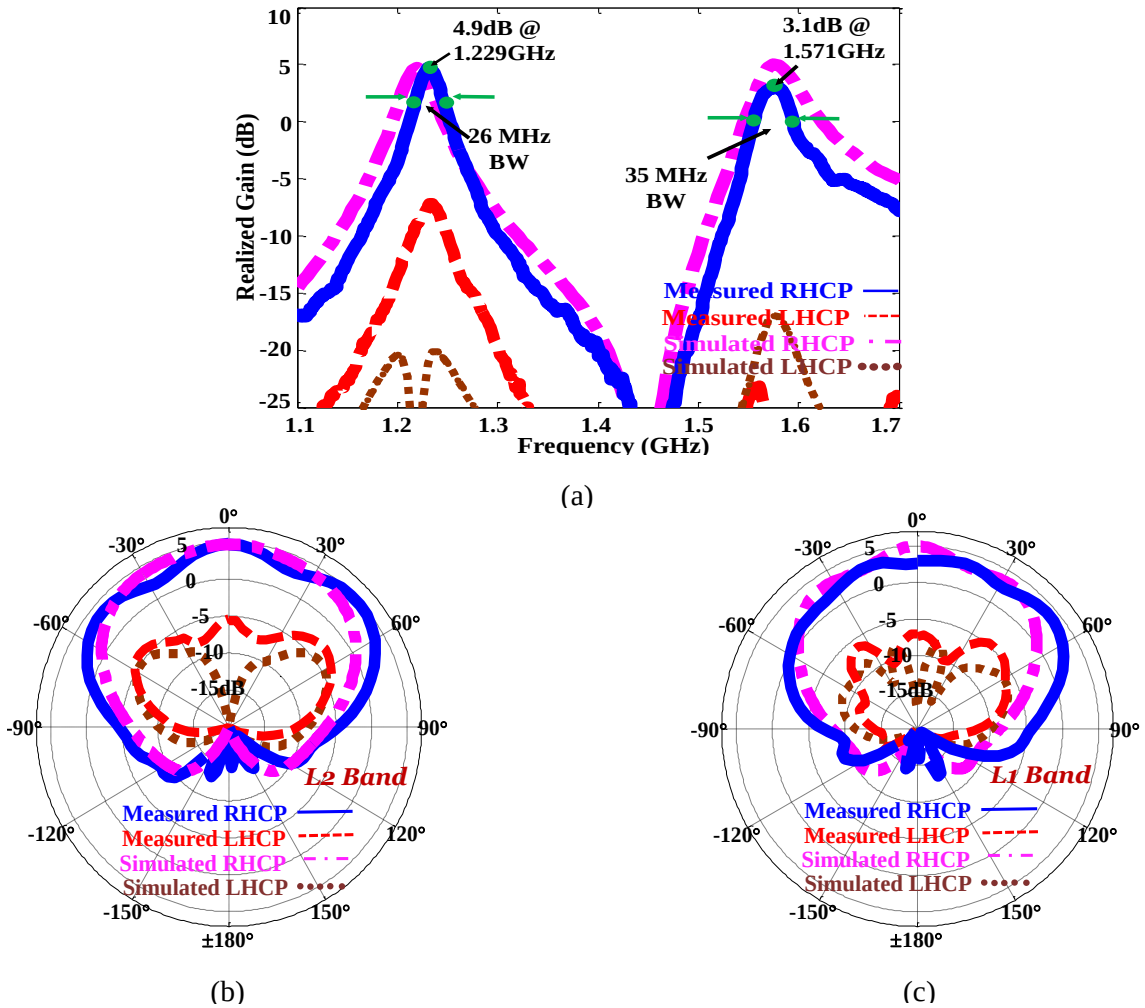

Figure 3.8: Simulated and measured. (a) Broadside RHCP and LHCP gains within the 1.1–1.7GHz band; Simulated and measured radiation patterns in the x-z plane at (b) L2 and (c) L1 bands.

tanδ=0.0022) substrate and consisted of 50Ω grounded co-planar waveguide (CPWG) lines, a 50Ω resistive termination (i.e. isolation port), a 50Ω coaxial probe (i.e. input), and a surface mount quadrature hybrid coupler (Anaren Microwave, Xinger-brand components, part#XC1400P-03S). The antenna was fed through vertical copper pins connected to the CPWG lines as depicted in Fig. 3.7(b).

Fig 3.8(a) presents the measured and simulated broadside RHCP and LHCP gains within the 1.1–1.7GHz band when the antenna was centered on a 24"×24" brass ground plane. For comparison purposes, the antenna design finalized over the infinite ground plane (see Fig 3.1(a))

was simulated over a large 24"×24"×0.025" finite ground plane and the results were superimposed with the measured data presented in Fig. 3.8. Due to the addition of the feed network and associated fabrication tolerances, the peak gains were observed at slightly different frequencies as compared to the measured S_{11} performance reported in Fig. 3.6(d). Specifically, the miniature dual-band CDL GPS antenna exhibited 4.9dB realized gain at 1229MHz and 3.1dB realized gain at 1571MHz with 26MHz and 35MHz 3dB realized gain bandwidths, respectively. The cross polarization levels at both bands were measured to be >10dB lower than the co-polarized gain. The measured increase in the L2 band cross polarized gain (as compared to simulated) can be attributed to the fabrication tolerances, inequalities in the pin heights, the ground plane shape and size. Fig.3.8 (b) and (c) demonstrate the measured and simulated x-z plane radiation patterns at the L2 and L1 bands, respectively. Due to the square shaped antenna and ground plane geometry, the measured radiation patterns in the y-z plane are almost identical to those in x-z plane and therefore not shown for brevity. The CDL GPS antenna operates with 82% and 72% measured radiation efficiencies at the L2 and L1 bands, respectively [65].

3.5. Concluding Remarks

A miniature dual-band CDL GPS antenna was presented. To achieve the goals of size miniaturization, high radiation efficiency, and proper spacing of the L2 and L1 resonances; the antenna layout simultaneously incorporated meandered lines, lumped capacitors, and volumetric reactive loadings. Specifically, an antenna design realized over 500mil thick Rogers TMM10i (ε_r=9.8) and fed with a CPWG based hybrid was shown to exhibit broadside peak RHCP realized gains of 4.9dB at L2 and 2.1dB at L1 bands with 26MHz and 35MHz 3dB realized gain bandwidths, respectively. This CDL antenna was shown to occupy 60% smaller size (1.1"×1.1" ~λ_0/8.8×λ_0/8.8 at L2) as compared to a traditional patch antenna fabricated on the same substrate.

CHAPTER 4: CIRCULARLY POLARIZED PRINTED ANTENNA MINIATURIZED USING COMPLEMENTARY SPLIT RING RESONATORS AND REACTIVE PIN LOADINGS[3]

4.1. Introduction

Small, low cost, and efficient antennas are becoming increasingly important to address the needs of advancing communication technologies. Due to their low profiles, high radiation efficiencies, and low costs; microstrip patch antennas are attractive but their footprints are large and limited by the electrical size of their cavity. It is therefore not surprising to see that many diverse miniaturization techniques have been investigated for their size reduction. For example, miniaturization by employing high permittivity [6] and permeability [8] materials as the antenna substrates are known to be effective but generally considered to increase fabrication costs. Folding and meandering the patch geometry [22-24, 66] is another size reduction technique, but can degrade the mechanical robustness of the design and radiation efficiency. Etching slots on the ground planes [34, 36] of patch antennas has been shown to result in size reduction, however, the method is known to reduce the front-to-back radiation ratio and is not suitable for certain conformal installations. Recently, several research groups have adopted engineered negative permeability (i.e. MNG) substrates made-up from periodic arrangements of spilt ring resonators (SRRs) as an alternative miniaturization technique [14-16]. However, the necessary vertical

[3]S. Gupta, M. Gokhan, 'Circularly polarised printed antenna miniaturised using complementary split-ring resonators and reactive pin loading," *IET Microwaves, Antennas and Propagation*, doi: 10.1049/iet-map.2014.0240.

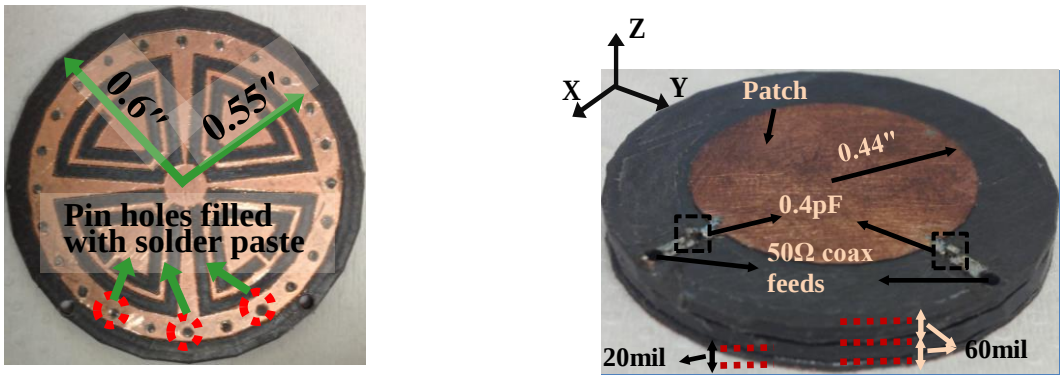

(a) (b)

Figure 4.1: Patch-CSRR fabricated prototype. (a) pin loaded CSRR metallization layer; (b) 3D view of the three layer antenna assembly.

alignment of the SRRs with respect to the antenna ground plane significantly increased the fabrication complexity and associated cost. More recently, inspired from the fact that periodic arrangements of complementary versions of split ring resonators (CSRRs) can generate an engineered negative permittivity (i.e. ENG) material [21], a new miniaturized patch has been realized by horizontally placing a CSRR between the ground and antenna metallization planes [5]. This antenna has been designed by utilizing a genetic algorithm optimization approach and can only radiate with linear polarization due to its rotationally asymmetric layout. This paper extends this antenna topology by utilizing multiple CSRR loadings within the patch cavity in order to realize a symmetric antenna layout capable of supporting circularly polarized radiation. The design is also carried out differently by resorting to a unit cell based parameter extraction method [58, 63, 67]. It is demonstrated that, the size of the antenna is determined by the overall area of the metallization in which the CSRRs are formed in. Therefore, an additional miniaturization technique based on reactive pin loading [68, 69] is utilized around the CSRR metallization (see Fig. 4.1) to provide additional size reduction beyond what can be accomplished with stand-alone CSRR loading. Specifically, an antenna exhibiting a diameter of 1.2″ ($\lambda_0/4$ @2.42GHz) is designed and experimentally shown to operate with measured 4.1dBic

broadside right hand circularly polarized (RHCP) gain with 1.1% $|S_{11}|$<-10dB bandwidth. As compared to a conventional patch antenna designed over the identical substrate stack-up, presented antenna is shown to exhibit 44% smaller diameter, implying a 75% footprint area reduction.

4.2. CSRR Loaded Circularly Polarized Antenna

Fig. 4.2(a) depicts the CSRR loaded antenna layout carried over the substrate stack-up depicted in Fig. 4.2(b). To enable circularly polarized radiation, the layout utilizes a cascade of four unit cells and exhibits 90^0 rotational symmetry. The antenna utilizes two metallization surfaces over an electrically large ground plane (modelled as infinitely large to reduce simulation time). Top metallization layer forms the patch and associated feed lines. The bottom metallization layer hosts a circular metallization pattern from which slots are etched out to form the CSRR unit cells. The antenna substrate is constructed from Rogers RT/Duroid 5880 (ε_r=2.2, tanδ=0.0009) by stacking up three layers, top to bottom, with thicknesses of 60mil, 60mil and 20mil, respectively. The CSRR metallization is 80mil (60mil+20mil) above the ground plane. The 20mil thick substrate is specifically introduced to isolate the 60mil layer from the ground plane as this layer will be later utilized in Section 4.3 to host the reactive pin loadings. Fig. 4.2(c) depicts the computational model of the unit cell (throughout the manuscript, Ansys HFSSv14 was utilized as the full-wave solver). Since CSRRs exhibit an electric field component normal to their metallization plane, the resonance frequency of the unit cell can be extracted by treating it as a two port network and computing the corresponding scattering parameters. For the unit cell dimensions given in Fig. 4.2(c), the resonance frequency is realized at 2.4GHz as shown in Fig. 4.2(d). These S-parameters also leads to an equivalent negative permittivity when the transmission/reflection based material extraction presented in [67] is utilized, and confirms the

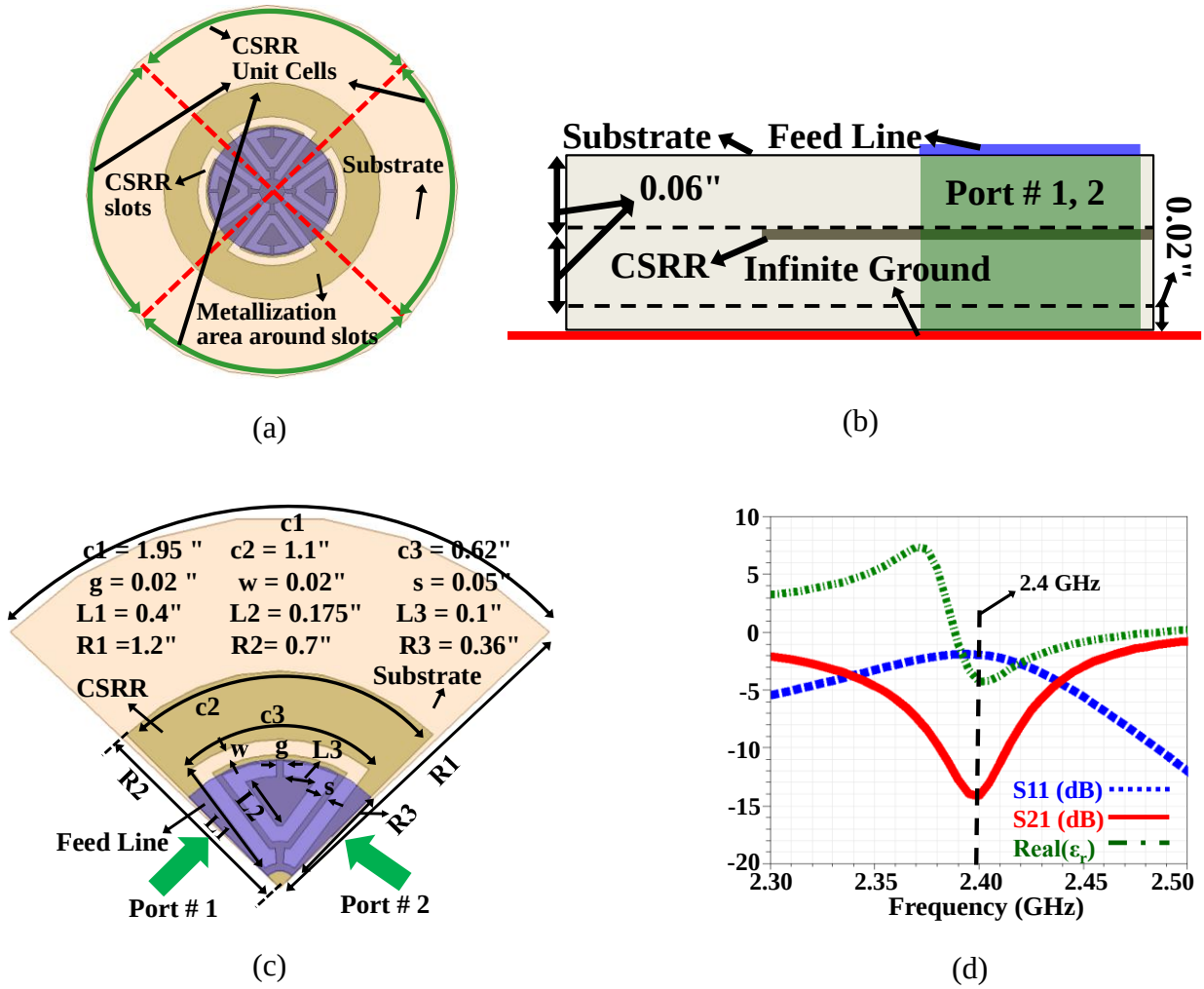

Figure 4.2: CSRR loaded patch antenna. (a) consisting of 4 circularly cascaded unit cells; CSRR Unit cell layout with its corresponding performance: (b) Side View and (c) Top View; (d) Simulated S-parameters and extracted permittivity (ε_r) of the unit cell.

epsilon negative nature of the periodic CSSR media. The unit cell design was carried out through the parametric studies. Qualitatively, an increase in the total slot lengths controlled by parameters L1, L2 and c3 decreases the resonance frequency. Narrowing the slot widths (w) results in lower resonance frequency as well. Radius of the bottom metallization layer (R2) plays a critical role in defining the resonance frequency of the unit cell. Specifically, smaller R2 value results in higher resonance frequency. On the contrary, with the increase in the radius of top metallization layer (R3), resonance frequency of the unit cell shifts up and vice-versa.

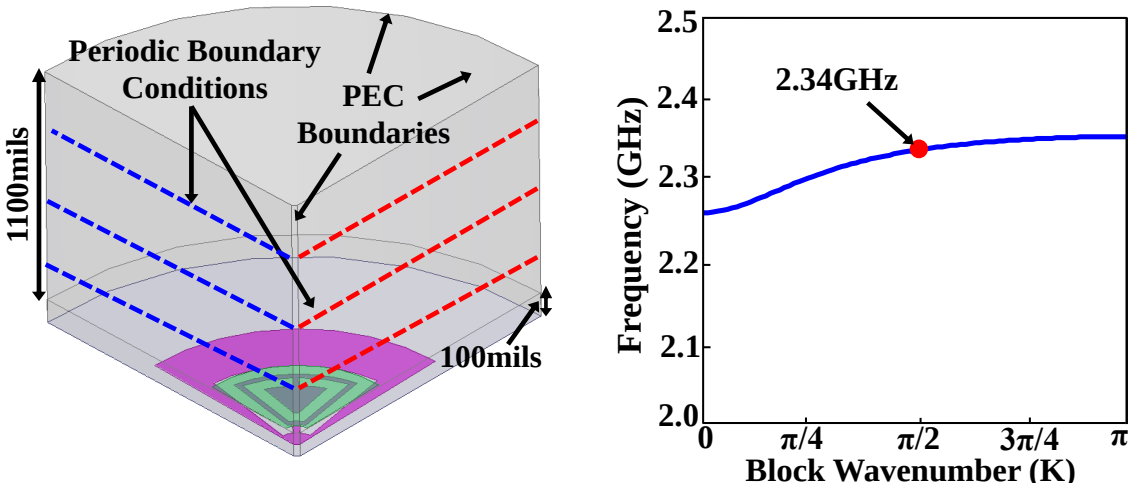

(a) (b)

Figure 4.3: Unit cell HFSS model and its dispersion diagram. (a) Computational model for eigenfrequency analysis; (b) Dispersion diagram of the unit cell.

In order to verify that the resonance frequency of the antenna consisting of four unit cells is associated with the resonance frequency of the unit cell extracted from the S-parameter analysis, a dispersion (K-ω) diagram analysis was also carried out in a similar fashion to the technique presented in [58]. As shown in Fig. 4.3(a), the unit cell depicted in Fig 4.2(c) was remodeled with periodic boundary conditions to set-up an Eigen frequency analysis. Fig. 4.3(b) presents the corresponding K-ω diagram demonstrating that waves propagating through the unit cell attain a total phase shift of $K=\pi/2$ at 2.34GHz, which is in close agreement with the frequency in Fig. 4.2(d). In a 4-unit cell periodic structure, this implies that the total phase shift, will be 2π hence satisfying the resonance condition for a closed loop. Consequently, one can resort to a dispersion diagram or material extraction based design technique to determine the resonance frequency of the proposed antenna structure.

Fig. 4.4(a) presents a comparison of the $|S_{11}|$ performances of a traditional patch antenna with the CSRR one (solid line). In order to provide a fair comparison, the size of the traditional patch is kept same as that of the CSRR loaded patch over an identical substrate arrangement. The

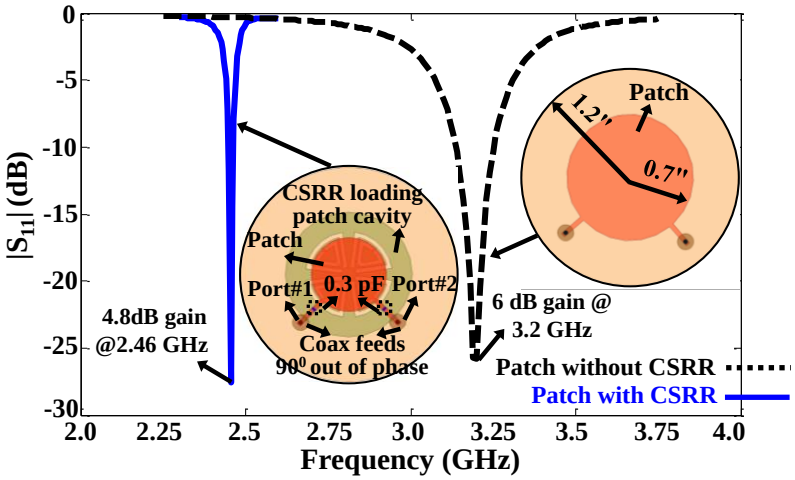

(a)

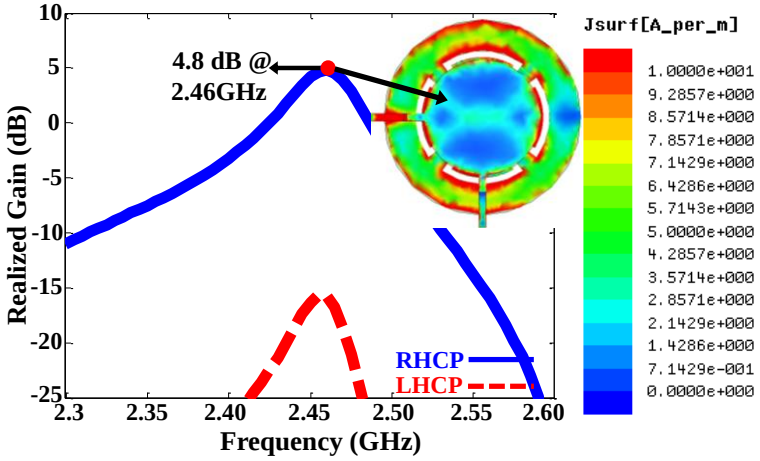

(b)

Figure 4.4: Simulated performance. (a) S_{11} of the CSRR loaded patch vs conventional patch; (b) Broadside realized RHCP-LHCP gains of the CSRR loaded patch.

CSRR loaded antenna is fed by two 90º out-of-phase 50Ω coaxial probes to achieve CP. In experimental verifications this is realized with a single surface mount quadrature hybrid coupler, as will be discussed in section 4.4. The impedance matching of the CSRR loaded patch is obtained by using series capacitors of 0.3pF when connecting the coax probes to the top metallization with strips. As shown in Fig. 4.4(a), the conventional patch antenna resonates at 3.2GHz as compared to 2.46GHz of the patch antenna loaded with CSRRs, therefore providing 25% electrically smaller design. However, this occurs at the expense of the bandwidth

performance (i.e. 3.4% vs. 0.8%). The CSRR loaded antenna operates with 4.8dBic realized RHCP gain at 2.46GHz and exhibits 74% radiation efficiency (see Fig. 4.4(b)). The cross-polarization gain is -20.5dB below the peak realized gain, implying an axial ratio of 1.7dB. The shift in the resonance frequency of the CSRR loaded patch antenna (Fig. 4.5(a-b)) as compared to the resonance frequency predicted by unit cell (Fig. 4.2(a-d)) and K-ω (Fig. 4.3(a-b)) analysis is due the inclusion of coaxial feed probes in the final antenna structure used in simulation. Nevertheless, a geometric parameter such as R2 can be utilized to precisely tune the antenna resonance if desired.

The surface current distributions on the metallization planes of the CSRR loaded antenna (see inset of Fig. 4.4(b)) demonstrate that both planes carry comparable amount of current. Therefore, the metallization size of the CSSR plane should not be ignored in evaluating the size reduction performance of the CSRR loadings as opposed to the comparison presented in [5]. The footprint diameter of the CSRR loaded antenna is 1.4" (~λ_0/3.5 @ 2.46GHz), whereas the diameter is only 0.88" (~λ_0/5.5 @ 2.46GHz) if the metallization disk area (shown in Fig. 4.2(a)) surrounding the slots of the CSRR is ignored. Hence, reducing the size of the CSRR metallization area (i.e. R2) is necessary for accomplishing an improved miniaturization performance.

4.3. Further Size Reduction with Reactive Loading Pins

To study the effect of reducing the CSRR metallization size on the antenna performance, computational studies were carried out by reducing down R2 from 0.7" to 0.55" in 25mil steps. As shown in Fig. 4.5(a), the resonance frequency shifted from 2.46GHz to 3GHz with an approximate linear rate of 3.6MHz/mil. The radiation efficiency of the antenna increased slightly from 74% to 78% due to reduction in ohmic losses associated with large conducting plate size.

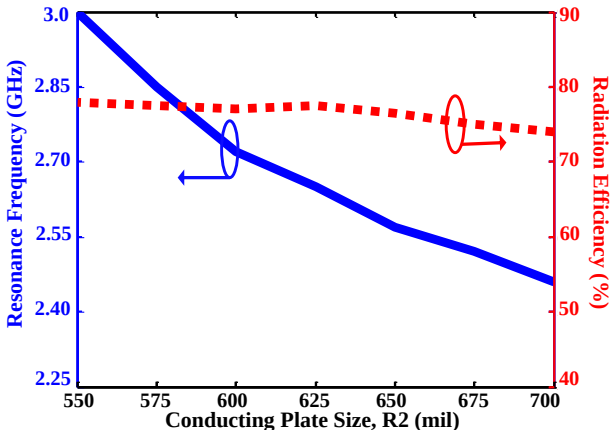

(a)

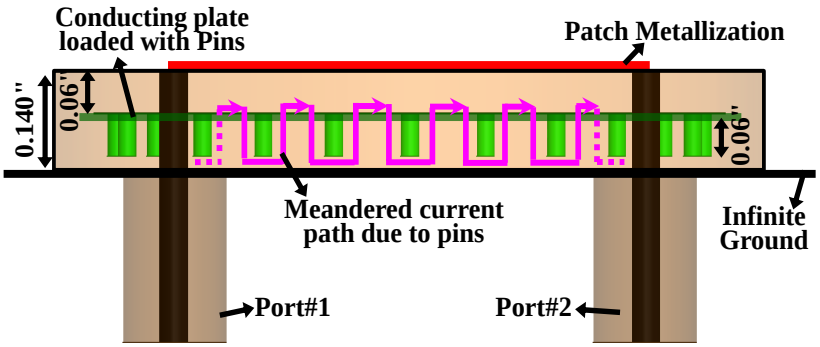

(b)

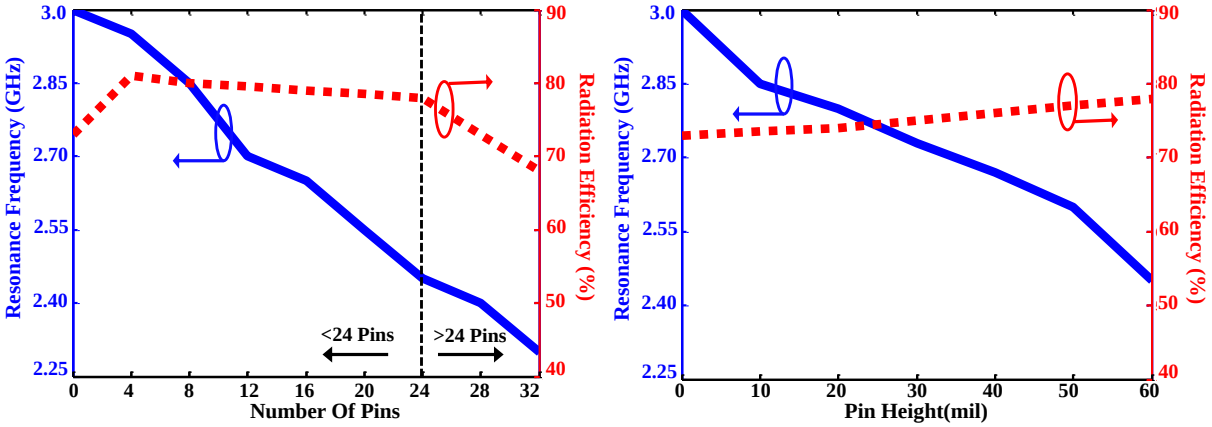

(c) (d)

Figure 4.5. Computational study on conducting plate size and pins. (a) Effect of reducing conducting plate size on resonance frequency and radiation efficiency; (b) Side view of the antenna over the reduced substrate with volumetrically loaded pins on CSRR metallization; Resonance frequency and radiation efficiency variance with (c) number of pins and (d) increasing pin height.

When the substrate size was also reduced down to barely fit the antenna footprint (i.e. R1=R2=0.55"), the radiation efficiency of the antenna got lowered from 78% to 73% due to increase in the current density across the CSRR and patch metallization layer, [68]. On the other hand, the substrate size reduction did not impact the resonance frequency.

To compensate for the increase in resonance frequency due to R2 reduction, we proceeded to investigate volumetrically loading the CSRR metallization with vertical conductive pins as was utilized in our recent work [68]. As shown in Fig. 4.5(b), the metallization disk area surrounding the CSRRs was loaded with N=24 60mil long pins having 31.5mil diameters (selected based on drilling tool availability). The pins were electrically connected to the CSRR metallization plane, but did not make connection with the ground plane. The pins support a current distribution that serves as an extension length for the surface current on the top of the CSRR metallization, thereby providing a meandered current path (see Fig. 4.5(b)) that resulted in lowering of the resonance frequency [68, 69]. The selection of the N=24 number of pins was based on the results of the computational parametric analysis depicted in Fig. 4.5(c). As the number of pins was increased from 0 to 32 in steps of 4 (to maintain the 90^0 rotational symmetry), the resonance frequency of the antenna shifted down from 3GHz to 2.3GHz. Although there was an initial increase in radiation efficiency from 73% to 81% when the antenna was loaded with only 4 pins, radiation efficiency slightly decreased down to 78% as the number of pins was increased from 4 to 24. This drop in radiation efficiency can be attributed to the ohmic losses added by the pins. As the number of pins is increased beyond 24, the decrease in radiation efficiency becomes more prominent. The antenna resonated at 2.45GHz for N=24 and this was selected for the final design and experimental verification. In the presented design, the pin lengths were fixed to 60mils in order to utilize a readily available substrate thickness for

convenient fabrication. Nevertheless, the sensitivity of the design with respect to the pin lengths were also investigated for N=24 case as depicted in Fig. 4.5(d).Specifically, it was observed that the resonance frequency almost decreased linearly with a rate of 9.1MHz/mil. In addition, it was also observed that the pin loadings increased the radiation efficiency from 73% to 78%. This is because pin loadings distribute the current volumetrically around the antenna structure [68].

4.4. Experimental Verification

An antenna prototype was fabricated with standard PCB manufacturing as shown in Fig. 4.1. The structure was realized using three layers of Rogers RT/Duroid (ε_r =2.2, tanδ = 0.0009) substrates with thicknesses of 60mil, 60mil, and 20mil as depicted in Fig. 4.1(b). The holes were filled with LPKF solder paste. The radiation performance measurements were taken in the anechoic chamber of the University of South Florida after integrating it with the feed network shown in Fig. 4.6(a). The feed network was implemented over a 25mil thick Rogers 6010.2LM (ε_r=10.2, tanδ=0.0022) substrate and consisted of 50Ω grounded co-planar waveguide (CPWG) lines, a 50Ω resistive termination (i.e. isolation port), a 50Ω coaxial probe (i.e. input), and a surface mount quadrature hybrid coupler (Anaren Microwave, Xinger- brand components,

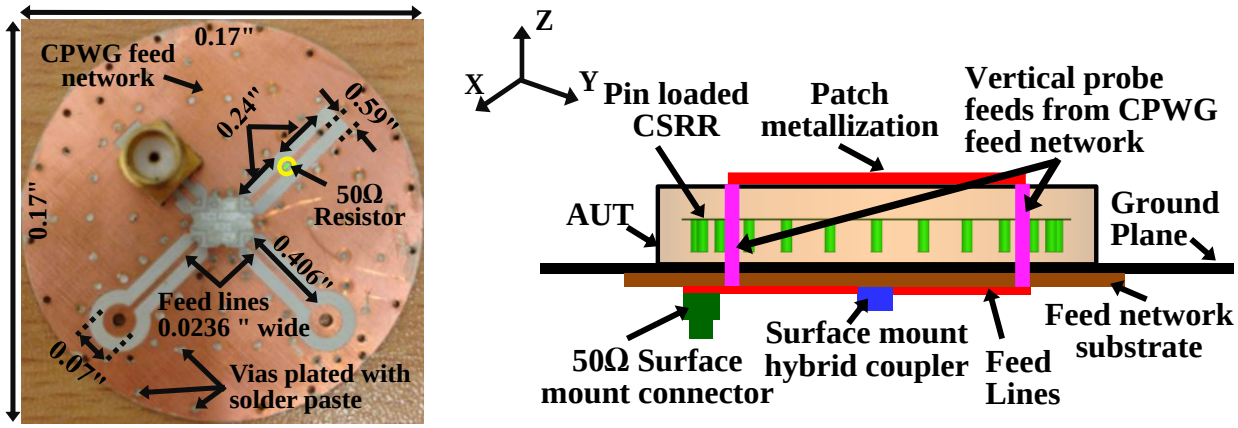

(a) (b)

Figure 4.6: Fabricated antenna feed structure. (a) Layout with dimensions; (b) Illustration of the feed mounting over the 24"×24"×0.025" brass ground plane.

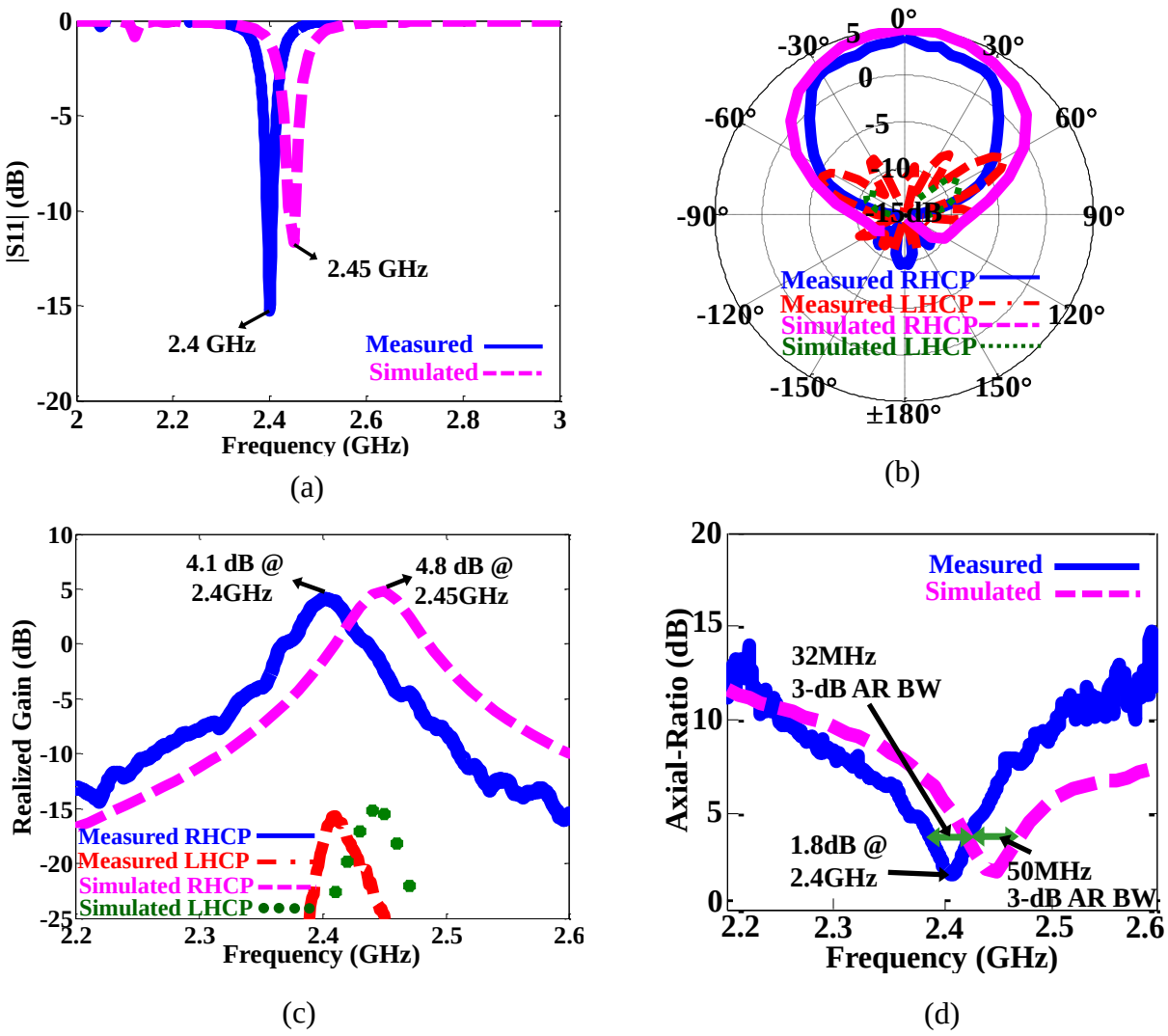

Figure 4.7: Simulated and measured performances. (a) $|S_{11}|$ (b) Realized gain patterns in the x-z plane (c) Broadside RHCP and LHCP realized gains (d) Axial ratio with 3dB BW.

part#1P603AS). The antenna was fed through vertical copper pins connected to the CPWG lines as depicted in Fig. 4.6(b). The measurements were taken on 24"×24"×0.025" brass ground plane. For comparison purposes, the antenna design finalized over the infinite ground plane (see Fig. 4.5(b)) was simulated over the selected finite ground plane and the corresponding results were superimposed with the measured data presented in Fig. 4.7. Fig. 4.7(a) depicts the return loss performance. Specifically, the fabricated prototype operates at 2.4GHz with 1.1% |S11|<-10dB bandwidth. This is in good agreement with the simulated 2.45GHz resonance frequency

and 0.8% bandwidth. The resonance shift can be attributed to thinning of the substrate layers due to the milling machine based fabrication. Fig.4.7 (b) demonstrates the measured and simulated x-z plane radiation patterns at 2.4GHz and 2.45GHz, respectively. Due to the 90^0 rotationally symmetric antenna and ground plane geometry, the measured radiation patterns in the y-z plane are almost identical to those in x-z plane, and therefore not shown for brevity. Fig 4.7(c) presents the measured and simulated broadside RHCP and LHCP gains. The prototype exhibited 4.1dBic

Table 4.1: Comparison of simulated antenna performances. Patch sizes in row# 2 & 3 is identical to the CSRR size of section 4.2 & 4.3, respectively.

Description	Resonance (GHz)	Realized Gain (dBic)	|S11|<-10dB BW (%)	Efficiency (%)
Conventional patch	3.2	6	3.4	95
Patch loaded with CSRRs	2.46	4.8	0.8	74
Conventional patch on reduced substrate size	4.31	7.5	3.0	90
Patch on reduced substrate size with pin loaded CSRRs	2.45	4.4	1.1	78

Table 4.2: Performance comparison of the proposed antenna with recently reported miniaturized CP antennas.

Antenna Structure	|S11|<-10dB BW (%)	3-dB AR BW (%)	Gain (dBi)	Efficiency (%)	Miniaturization (%)	Overall volume (λ_0^3)
This work	1.1	1.3	4.4	70	44	0.246 x 0.246 x 0.03
[70]	4.6	1.46	2.98	-	39	0.28 x 0.28 x 0.025
[71]	1.04	1.68	-2	-	34	0.27 x 0.27 x 0.024
[72]	2	0.7	3.95	-	10	0.27 x 0.27 x 0.013
[73]	1.98	0.66	3.8	-	10	0.273 x 0.273 x 0.013
[74]	5.2	1.6	3.41	-	18.5	0.292 x 0.292 x 0.031
[75]	3.85	1.5	0.8	-	8	0.281 x 0.281 x0.0125
[76]	2.5	0.5	4.3	-	6	0.288 x 0.288 x 0.012

peak realized gain at 2.4GHz. The cross polarization level is ~19dB lower than the co-polarization level. Fig 4.7(d) depicts the measured vs simulated axial ratio. The measured prototype exhibits an axial ratio of 1.8dB @ 2.4GHz with 3-dB axial ratio BW of 1.3%. The antenna operates with 70% (Vs. 78% simulated @ 2.45GHz) measured radiation efficiency at 2.4GHz [65]. The antenna has an overall diameter of 1200mil ($\lambda_0/4$ @ 2.42GHz). This is 44% electrically small as compared to a traditional patch antenna that exhibits identical diameter as that of pin loaded CSRR. The traditional patch antenna operates at 4.31GHz over the identical substrate configuration. Table 4.1 summarize the simulated antenna performances of the reported antennas and provide a comparison with the conventional patch antennas exhibiting the identical size and substrate configuration. In Table 4.2, the measured performance of the miniaturized antenna with pin loaded CSRRs is compared to the recently reported compact CP antennas. It is observed that the presented antenna offers a higher miniaturization level and operates with comparable gain, efficiency, and axial ratio bandwidth performance. Due to the higher miniaturization level, the |S11|<-10dB bandwidth performance is relatively lower.

4.5. Concluding Remarks

A circularly polarized printed antenna miniaturized by utilizing a combination of complementary split ring resonators (CSRR) and reactive pin loadings was presented. Specifically, the reactive pin loadings were shown to provide an enhancement for the CSRR loading based antenna miniaturization without degrading the radiation efficiency performance. Specifically, a 2.4GHz antenna design was carried out and experimentally verified to operate with 4.1dBic measured broadside RHCP realized gain, 70% radiation efficiency, and 1.1% |S11|<-10dB bandwidth. The antenna has an overall diameter of 1200mil ($\lambda_0/4$ @ 2.4GHz) and

its diameter is 44% smaller as compared to its traditional counterpart built over the identical substrate configuration.

CHAPTER 5: VOLUMETRICALLY LOADED MINIATURIZED PRINTED FILTERS

5.1. Introduction

The demand for communication systems that are compact, lighter, portable and less complex calls for small, low loss and low-cost RF filters. It is not therefore surprising to see that many techniques have already been proposed to realize small RF filters. Filters deigned with LTCC and laminate waveguides have been thoroughly investigated in [37-43]. These kinds of filters are large in size and costly as compared to microstrip filters. Generally, microstrip filters are based on traditional half and quarter wavelength resonators. In [41, 44, 45], size of the filters has been reduced by using quarter-wave transformers. Although, these filters demonstrate good performance, their structures are complicated due to use of folding topology and mass of shorted vias. Reference [77] proposed compact bandpass filters using half-wavelength resonators. These filters do not require vias, but their sizes are larger than the filters proposed in [41, 44, 45].

Recently, filters using sub-wavelength 1-D rectangular cavity resonators have been implemented [78-81]. These rectangular cavities are composed of double positive (DPS) and double negative (DNG) layers. In [82], this approach was further extended by implanting the filter design using 3-D rectangular cavity resonators as compared to the ones used in [78-81]. These 3-D cavities are made up of a DPS and μ- negative material (MNG). Although the size of the filter was reduced, the design has some drawbacks due to its increased fabrication complexities and high insertion loss (~>-3dB). Lumped elements are often used as a miniaturization technique in filters [46-48]. However, lumped elements at microwave

frequencies have very poor quality factors, thereby, exhibiting high insertion loss, poor out-of-band rejection and undesirable self-resonance. Miniaturized printed microstrip transmission line filters are very popular due to its planar structure, easy fabrication and simple synthesis process. In the past, several filter designs have been proposed in this direction. In [83], a BPF filter is implemented using multilayer synthetic quasi-TEM TLs. The proposed approach provides good miniaturization but has a drawback due to high insertion loss (2.46dB @ ~2.5GHz).

As an alternative to above techniques, in this Chapter, we study the performance of the volumetric pin loading technique (introduced in Chapter 3 and 4 for antenna applications) in design and performance of miniaturized RF filters. Specifically, section 5.2 considers a volumetrically loaded microstrip line and provides a study of phase shift attained due to pins within the presence of mutual coupling effects. The variation in unloaded quality factor is investigated as a volumetrically loaded microstrip line resonator is miniaturized with addition of pins. Section 5.3 provides a pin loaded filter design example with its performance results. In this example, the proposed concept of miniaturization has been implemented for half wavelength bandpass hairline filters. The miniaturized filter design has a footprint size of $\lambda_0/17\times\lambda_0/9$ @ 2GHz and is 45% smaller than its traditional counterpart.

5.2. Mutual Coupling Between the Pins

To understand the variations in quality factor and the phase shift as a function of geometric arrangements of the pins, computational studies were carried out using Agilent ADS momentum. Fig. 5.1(a), depicts a $\lambda_g/2$ (@ 2GHz) pin loaded microstrip line resonator implemented over Rogers RT/D 6006 substrate, ($\varepsilon_r = 6.15$, $\tan\delta=0.0019$, thickness = 50mil). The resonator can be modeled as a periodic structure consisting of unit cells. As an initial study, the

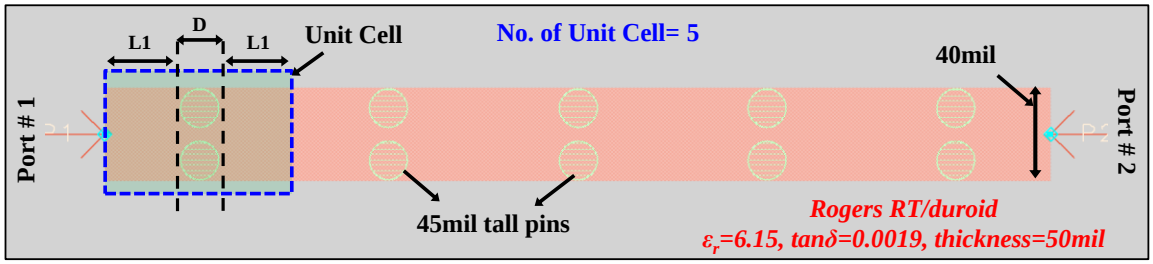

(a)

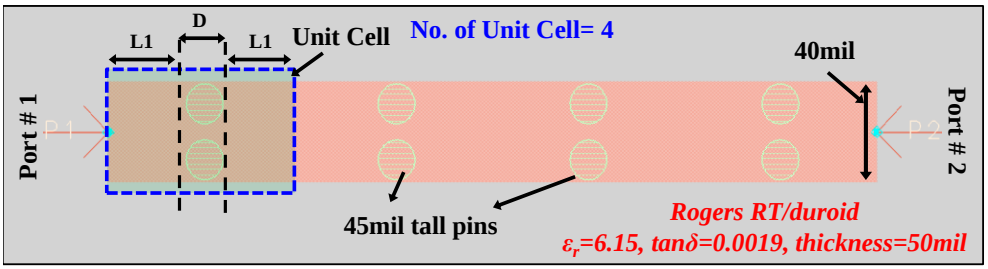

(b)

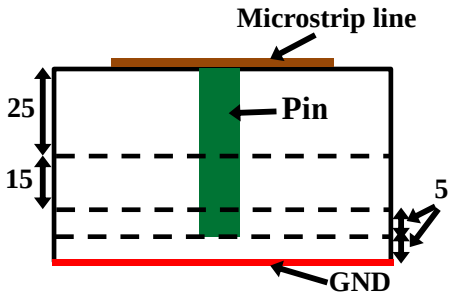

(c)

Figure 5.1: Pin loaded microstrip line. (a) 5 unit cell; (b) 4 unit cell; (c) substrate stack up with dimensions in mil.

resonator shown in Fig. 5.1(a) was divided into 5 unit cells (abbreviated as UC). Each UC consists of a microstrip line section loaded with a pair of pins (length D) and two adjacent microstrip line sections (each of length L1). Based on the study of current distribution on microstrip line, the pins were positioned at its outer edges. The height of the pins was chosen to be 45mil (diameter, D = 15mil) and was kept constant throughout the study. It should be noted that the pins are electrically connected to the top metallization and does not touch the ground plane by being5 mil above (see substrate stack up Fig. 5.1(c)). This substrate stack up

configuration was chosen based upon the availability of the substrate thicknesses and was kept the same throughout our discussion. The aim here is to study the phase shift provided by the pins of a single UC in the presence of coupling as the lengths of the microstrip lines (i.e. L1 in UC) are reduced gradually. Fig. 5.1(b), depicts pin loaded microstrip line with identical width, pin height and substrate configuration as that of Fig. 5.1(a), except it consists of 4 UCs. In order to obtain the phase shift of a single UC, S-parameter simulation of structures in Fig. 5.1(a) and (b) were carried out. This S-parameter data was then converted to ABCD parameters to obtain the ABCD parameters of a single UC in the presence of coupling as follows:

$$[ABCD]_{UC=1} = \text{inv}([ABCD]_{UC=4}) * [ABCD]_{UC=5} \quad (5.1)$$

where, $[ABCD]_{UC=1}$ = ABCD parameters of a single UC in the presence of coupling

$[ABCD]_{UC=4}$ = ABCD parameters of pin loaded microstrip line with 4 UCs

$[ABCD]_{UC=5}$ = ABCD parameters of pin loaded microstrip line with 5 UCs

The ABCD parameters of a single UC obtained through equation (5.1) was converted into S-parameters. These S-parameters was then used to calculate the phase provided by one UC in the presence of coupling using the following equation:

$$\Phi_{UC=1} = 2*\Phi_{L1} + \Phi_{pin}$$

$$\text{or,} \quad \Phi_{pin} = \Phi_{UC=1} - 2*\Phi_{L1} \quad (5.2)$$

where, $\Phi_{UC=1}$ = phase shift due to one UC in the presence of coupling

Φ_{L1}= phase shift due to microstrip line (calculated using ADS LineCal)

Φ_{pin} = phase shift due to pins in the presence of coupling

Fig. 5.2, shows the phase shift provided by the pins (of one UC) as the length of the microstrip lines (L1) is reduced. As can be seen, the phase shift due to pins decreases as the length of the microstrip line is reduced. This is due to the increase in mutual coupling between the adjacent UCs as the microstrip line length L1 is reduced. However, the phase of the pins remains almost

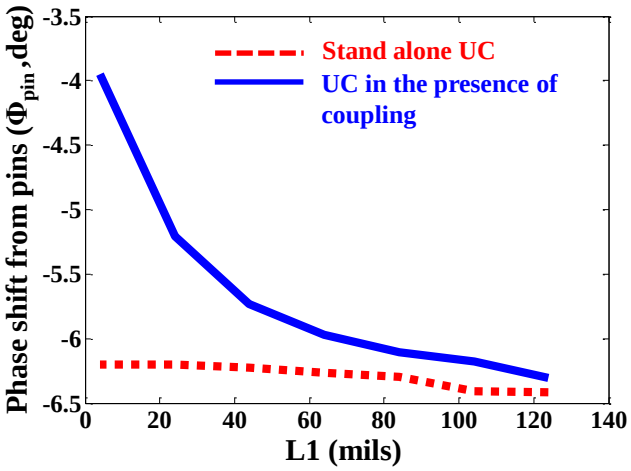

Figure 5.2: Phase shift of a single UC in the presence and absence of coupling. The length of the pin is 45mil and is kept constant.

constant in the absence of coupling (standalone case), as shown in Fig. 5.2. This implies that miniaturization offered by including more pins within a half wavelength open ended microstrip line resonator is going to saturate due to the mutual coupling between the pins as the phase shift coming from the pins will decline with more loading density.

Consequently, further investigations were carried out to study the effect of mutual coupling on the miniaturization percentage of the resonator and its unloaded quality factor. These computational studies were carried out using Ansoft HFSS. Fig. 5.3(a), depicts a $\lambda_g/2$ resonator (@2GHz) with 5 unit cells on Rogers RT/D 6006 substrate, (ε_r = 6.15, tanδ=0.0019, thickness = 50mil). The resonator was fed through input feed lines (5mils away from resonator) via capacitive coupling. The aim of this study is to investigate the maximum miniaturization that can be achieved by adding pin loaded UCs without increasing the physical size of the resonator and degrading its quality factor. These computational studies were carried out for two cases with pin diameter of 15mil and 5mil. Fig. 5.3(b, c), depict the total length of the resonator and its corresponding unloaded quality factor (Q_{UL}) versus the size of UCs used to resonate the structure at 2GHz. As the size of the UCs is reduced (i.e. by decreasing L1), the resonance frequency of

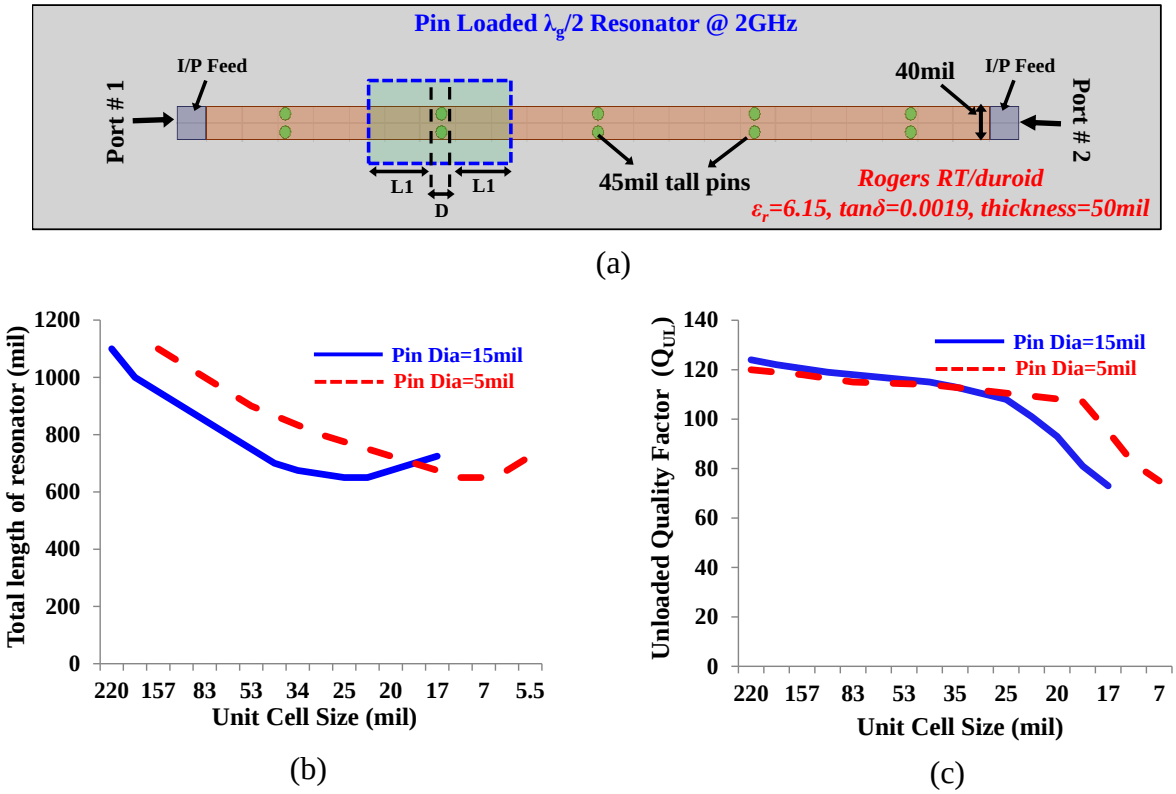

Figure 5.3: Pin loaded microstrip line $\lambda_g/2$ resonator. (a) with 5 UCs; Unit cell size for pin diameter of 15mil and 5mil: (b) vs total length of resonator; (c) vs unloaded quality factor of the resonator.

the resonator shifts to a higher frequency. This shift in frequency can be compensated by increasing the number of UCs of smaller size, see Fig. 5.3(b). However, after a certain size of UC (UC size = 35mil for pin diameter = 15mil) the resonance frequency of the resonator cannot be tuned to 2GHz without increasing its physical size. This is due the increase in mutual coupling between the adjacent UCs which leads to degradation of phase shift provided by the pins, as mentioned before. Also, it was observed that the Q_{UL} of the resonator decreases as the size of the resonator is decreased. This is because smaller size resonators (say 1000mil) incorporates more UCs as compared to larger size resonators (say 1100) which leads to higher copper loss associated with pins.

5.3. Pin Loaded Microstrip Line Filter Design

As a design example, half wavelength bandpass hairline was chosen. Fig. 5.4(a, b), depicts a traditional and a pin loaded half wavelength bandpass hairline five pole filter with Chebyshev lowpass filter response @ 2GHz. The design parameters of the filter are as follows [84]:

$$Q_{e1}=g_0*g_1/FBW, \quad Q_{en}=gn*g_{n+1}/FBW$$

$$M_{i,i+1} = FBW/\sqrt{g_i * g_{i+1}} \quad \text{, for i=1 to n-1}$$

$$Q_{e1} = Q_{e5} = 5.734$$

$$M_{1,2} = M_{4,5} = 0.16$$

$$M_{2,3} = M_{3,4} = 0.122$$

where, Q_{e1} and Q_{e5} = external quality factor of resonators at the input and output

$M_{i,\,i+1}$ = coupling coefficients between i and i+1 resonator, for i=1 to n-1

The filter is designed over Rogers RT/D 6006, ε_r = 6.15, tanδ=0.0019 with a substrate size of ~1.1"×8.7"×0.05" (~λ_0/5.5×λ_0/7×λ_0/120 @ 2GHz). The line width of the hairpin resonators was chosen to be 40mil and separation of 40mil between the two arms, as shown in Fig. 5.4(a, b). The spacing (S) between the adjacent resonators was chosen by calculating the coupling coefficients (M) using full wave EM simulation [84]. Fig. 5.4(c), shows the coupling coefficient of the traditional and the pin loaded hairline filter against the spacing (S). As the coupling coefficient decreases with increasing the separation (S), indicates the hairpin resonators have mixed coupling [84]. The filter is designed to have tapped line input and output. The width (73mil) of the tapped line is chosen such that it matches the terminating port impedance Z_0=50Ω. The tapping location is determined through the external quality (Q_e) factor analysis at the

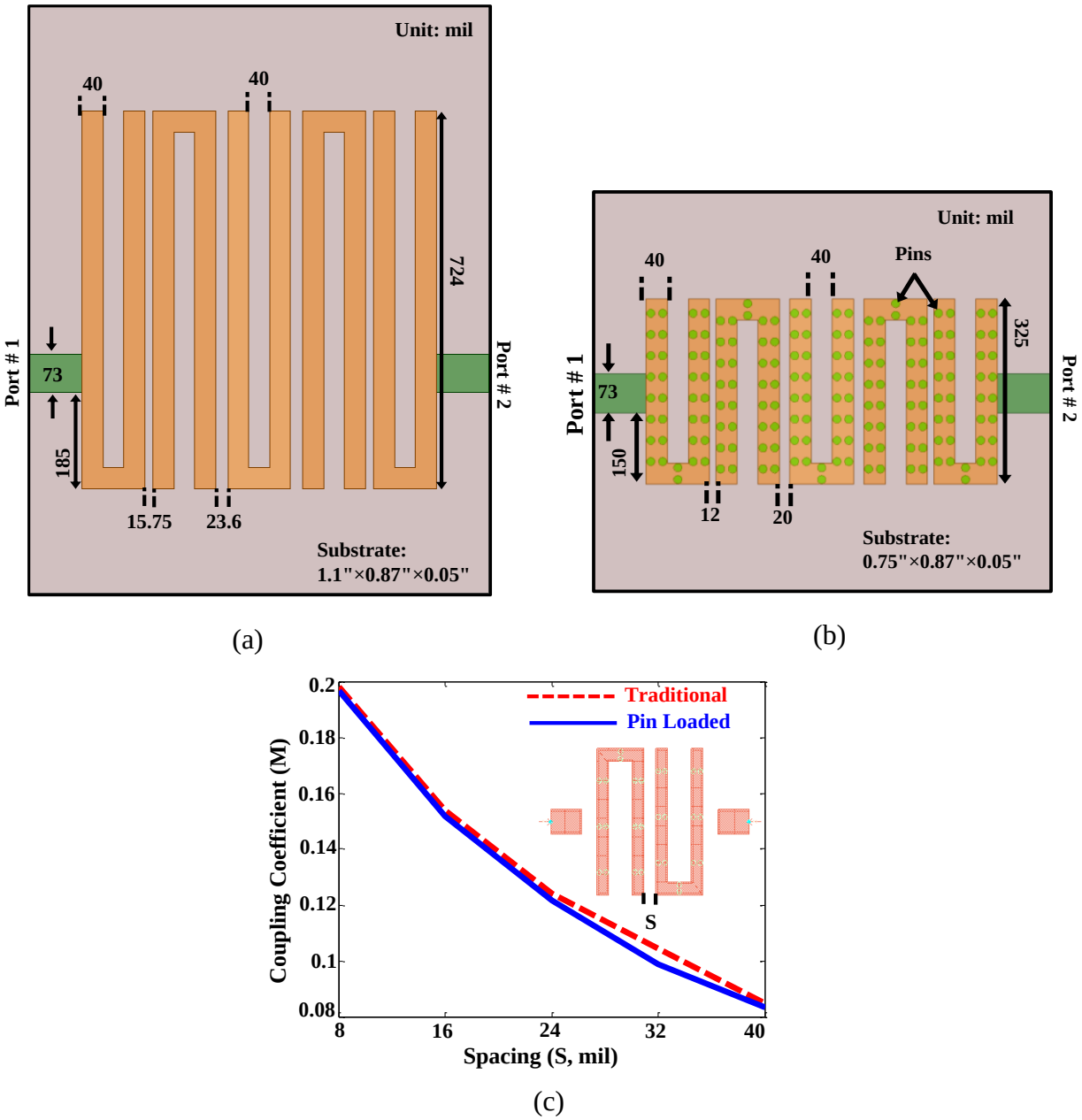

Figure 5.4: 5 pole, Chebyshev hairline filter. (a) Traditional; (b) Pin loaded hairline filter consisting of 17 UCs; (c) Coupling coefficients (M) vs spacing (S) between the adjacent resonators.

input and output resonators. Based on our computational studies in the section 5.2, the length of the resonator was chosen to be 700mil. Each resonator consists of 17 UCs (based on study of Fig. 5.3 (b, c)) with pin length of 45mil and diameter=15mil. The footprint metallization is etched over the Rogers RT/D substrate of size ~$\lambda_0/8\times\lambda_0/7\times\lambda_0/120$ @ 2GHz. Fig. 5.5 (a)-(d),

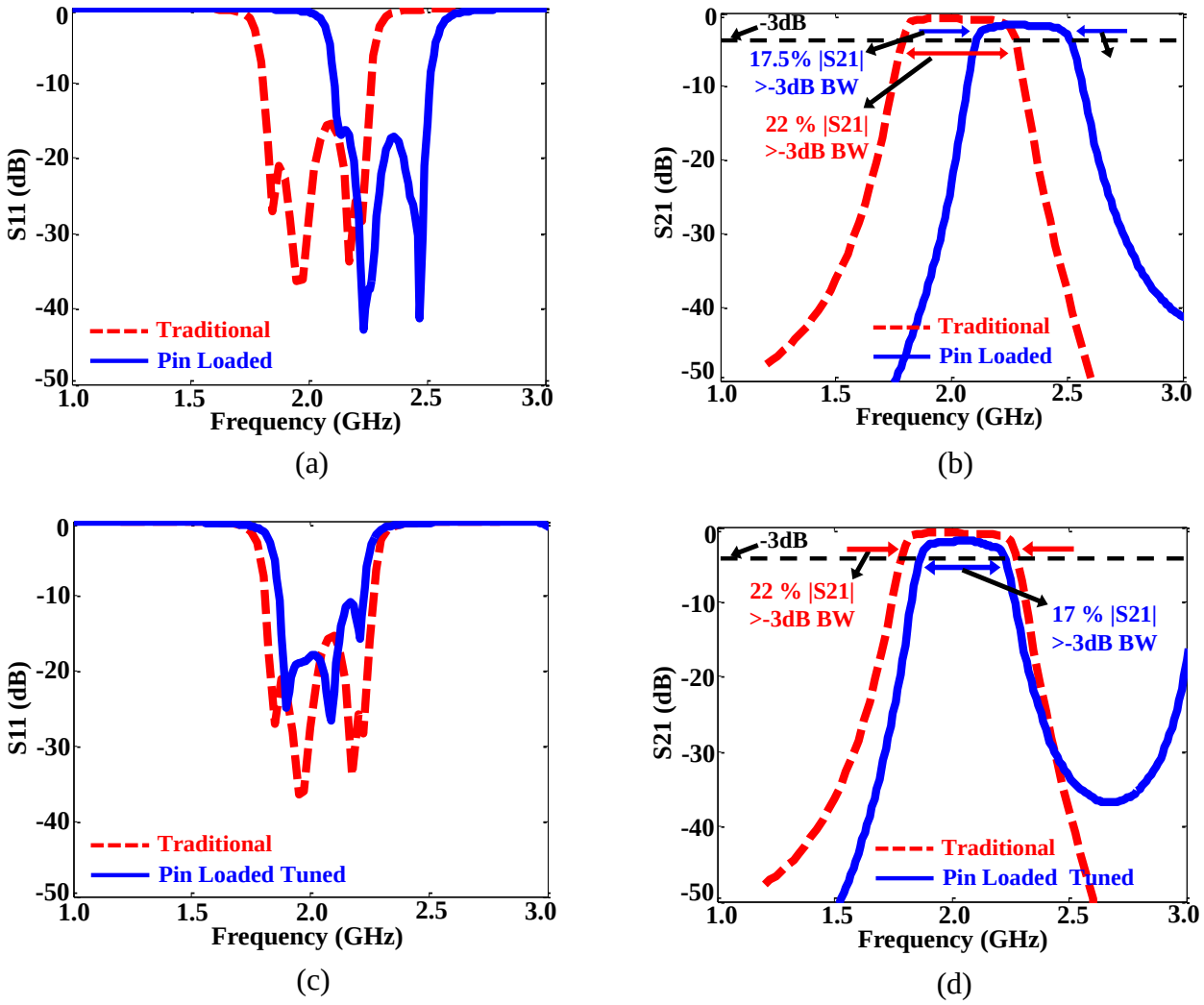

Figure 5.5: Performance comparison of pin loaded hairline and traditional filters. (a) $|S_{11}|$; (b) $|S_{12}|$; Tuned pin loaded hairline filter vs. traditional microstrip line filter performances (c) $|S_{11}|$ and (d) $|S_{12}|$.

shows a comparison of simulated return and insertion loss of traditional and pin loaded hairline filters. The proposed filter has an insertion loss of 1.5dB as compared to 1dB for traditional microstrip line filter. This increase in insertion loss could be attributed to the metallic loss associated with the pins. The length of the pin loaded hairpin resonator is ~700mil as compared to ~1500mil for its conventional microstrip line counterpart. However, it has 17.5% (@2.3GHz) >-3dB $|S_{21}|$ bandwidth as compared to 22% for traditional microstrip line filter. The S_{11} performance of the filters are in well agreement, however, there is shift in frequency (~0.2GHz)

in the passband. This shift in frequency can be compensated by increasing the length of resonators by adding two pin loaded UC of each length ~50mil, see Fig. 5.5(c, d). However, there is drop in >-3dB $|S_{21}|$ bandwidth from 17.5% to 17%. The pin loaded filter has 45% smaller footprint size (~$\lambda_0/16\times\lambda_0/9$ @ 2GHz) as compared to conventional microstrip line filter. The unloaded quality factor (Q_{UL}) of the pin loaded hairline filter is calculated to be 100 as compared to 140 for its traditional counterpart. However, the Q_{UL} of the hairline filter can be improved by increasing microstrip line width of the resonators. The Q_{UL} increased from 100 to 130 when the microstrip line width is increased from 40mil to 80mil.

5.4. Concluding Remarks

The design and performance evaluation of pin loaded microstrip line hairline filter was presented. The presented filter has a footprint size of ~$\lambda_0/16\times\lambda_0/9$ @ 2GHz and is 45% smaller than a conventional microstrip line filter. The design exhibited 17% $|S_{21}|$ <-3dB fractional BW with insertion loss of 1.5dB and computed Q_{UL} of 100. A higher Q_{UL} can be obtained by increasing the width of pin loaded resonator. A study of mutual coupling between the pins and its effect on the phase shift was carried out. A decrease in the phase shift provided by the pins is observed as the pins are brought closer to each other due to increase in mutual coupling.

CHAPTER 6: FUTURE WORK

The continuous demands for miniaturized GPS antenna arrays demands smaller antenna elements. Also, more antenna elements are desirable in order to obtain better array performance in terms of gain and signal strength. In order to obtain a smaller GPS antenna, the proposed CDL GPS antenna proposed in chapter 3 can implemented on higher permittivity substrates. Fig. 6.1 (a), depicts a CDL GPS L2-L1 band antenna implemented on a ceramic substrate 0.8"×0.8"×0.5", ε_r=25, tanδ=0.0002. The antenna has a footprint size of 0.75"×0.75"×0.50" (~λ_0/13 × λ_0/13) @L2 band. This is achieved by simultaneously implementing the design on high permittivity substrate and volumetrically loading the inner loop with vertical pins in addition to outer loop. Specifically, the CDL GPS antenna on higher contrast substrate is 50% smaller than the design implemented on ε_r=9.8 (presented in chapter 3). Fig. 6.1(b), shows the broadside RHCP-LHCP gains of the design simulated over an infinite ground plane. The miniature dual-band CDL GPS antenna exhibited 2.4dB realized gain at 1227MHz and 3dB realized gain at 1575MHz with 35MHz 0dB realized gain bandwidths, respectively. The cross polarization levels at both bands are 20dB lower than the co-polarized gain, indicating good CP. The antenna operates with 80% and 75% radiation efficiencies at L2 and L1 band, respectively.

The miniaturized patch antenna loaded (chapter 4) with CSRR operates in ISM and radiates with CP. The performance of the antenna can be further extended by making it to be multi-band by etching slots on the patch metallization. However, achieving simultaneous impedance matching at all bands could be a potential challenge to the designer. The filter

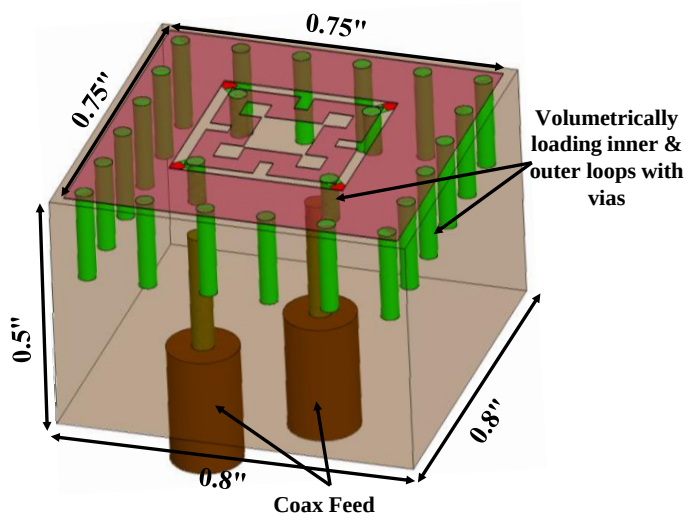

(a)

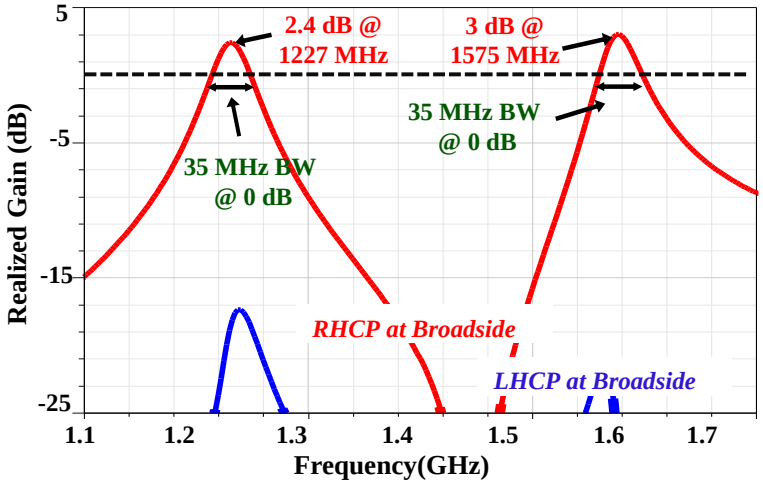

(b)

Figure 6.1: CDL GPS antenna on higher permittivity substrate. (a) Simulation model with layout dimensions; (b) Simulated broadside RHCH-LHCP gains.

presented in chapter 5 involves use of vertical pins for miniaturizing its size. Further, miniaturization can be obtained by implementing the design on high contrast substrate. In addition, the design can be made versatile by making it tunable. This can be achieved by integrating an active element to it, such as varacter diode. Also, resorting to liquid metal instead of metallic pins could be an option to obtain tunability [85, 86].

REFERENCES

[1] A. K. Skrivervik, Zu, x, J. F. rcher, O. Staub, and J. R. Mosig, "PCS antenna design: the challenge of miniaturization," *Antennas and Propagation Magazine, IEEE,* vol. 43, pp. 12-27, 2001.

[2] K. L. Wong, "Compact and Broadband Microstrip Antennas. Hoboken," *NJ: Wiley,* 2002.

[3] R. Waterhouse, "Small microstrip patch antenna," *Electronics Letters,* vol. 31, pp. 604-605, 1995.

[4] R. Porath, "Theory of miniaturized shorting-post microstrip antennas," *Antennas and Propagation, IEEE Transactions on,* vol. 48, pp. 41-47, 2000.

[5] R. O. Ouedraogo, E. J. Rothwell, A. R. Diaz, K. Fuchi, and A. Temme, "Miniaturization of Patch Antennas Using a Metamaterial-Inspired Technique," *Antennas and Propagation, IEEE Transactions on,* vol. 60, pp. 2175-2182, 2012.

[6] L. Byungje and F. J. Harackiewicz, "Miniature Microstrip Antenna with a Partially Filled High-Permittivity Substrate," *Antennas and Propagation, IEEE Transactions on,* vol. 50, pp. 1160-1162, 2002.

[7] D. H. Schaubert, D. M. Pozar, and A. Adrian, "Effect of microstrip antenna substrate thickness and permittivity: comparison of theories with experiment," *Antennas and Propagation, IEEE Transactions on,* vol. 37, pp. 677-682, 1989.

[8] I. S. Nefedov, A. C. Tarot, and K. Mahdjoubi, "Wire Media - Ferrite Substrate for Patch Antenna Miniaturization," in *Antenna Technology: Small and Smart Antennas Metamaterials and Applications, 2007. IWAT '07. International Workshop on*, 2007, pp. 101-104.

[9] Z. Yijun, C. Chi-Chih, and J. L. Volakis, "Single-fed Circularly Polarized Antenna Element With Reduced Coupling for GPS Arrays," *Antennas and Propagation, IEEE Transactions on,* vol. 56, pp. 1469-1472, 2008.

[10] Z. Yijun, C. Chi-Chih, and J. L. Volakis, "Dual Band Proximity-Fed Stacked Patch Antenna for Tri-Band GPS Applications," *Antennas and Propagation, IEEE Transactions on*, vol. 55, pp. 220-223, 2007.

[11] C. ShiChai, L. GuangCong, C. XiangYu, L. TingFen, L. XiangGuo, and D. ZhiQi, "Compact Dual-Band GPS Microstrip Antenna Using Multilayer LTCC Substrate," *Antennas and Wireless Propagation Letters, IEEE,* vol. 9, pp. 421-423, 2010.

[12] R. W. Ziolkowski and A. Erentok, "Metamaterial-based efficient electrically small antennas," *Antennas and Propagation, IEEE Transactions on,* vol. 54, pp. 2113-2130, 2006.

[13] J. Peng and R. W. Ziolkowski, "Multi-Frequency, Linear and Circular Polarized, Metamaterial-Inspired, Near-Field Resonant Parasitic Antennas," *Antennas and Propagation, IEEE Transactions on,* vol. 59, pp. 1446-1459, 2011.

[14] H. Mosallaei and K. Sarabandi, "Design and Modeling of Patch Antenna Printed on Magneto-Dielectric Embedded-Circuit Metasubstrate," *Antennas and Propagation, IEEE Transactions on,* vol. 55, pp. 45-52, 2007.

[15] F. Bilotti, A. Alu, and L. Vegni, "Design of Miniaturized Metamaterial Patch Antennas With μ -Negative Loading," *Antennas and Propagation, IEEE Transactions on,* vol. 56, pp. 1640-1647, 2008.

[16] A. Alu, F. Bilotti, N. Engheta, and L. Vegni, "Subwavelength, Compact, Resonant Patch Antennas Loaded With Metamaterials," *Antennas and Propagation, IEEE Transactions on,* vol. 55, pp. 13-25, 2007.

[17] C. Caloz and T. Itoh, "Electromagnetic Metamaterials: Transmission Line Theory and Microwave Applications," *Hoboken, NJ: Wiley-IEEE Press,* 2005.

[18] M. A. Antoniades and G. V. Eleftheriades, "A Folded-Monopole Model for Electrically Small NRI-TL Metamaterial Antennas," *Antennas and Wireless Propagation Letters, IEEE,* vol. 7, pp. 425-428, 2008.

[19] K. M. K. H. Leong, L. Cheng-Jung, and T. Itoh, "Compact Metamaterial Based Antennas for MIMO Applications," in *Antenna Technology: Small and Smart Antennas Metamaterials and Applications, 2007. IWAT '07. International Workshop on*, 2007, pp. 87-90.

[20] F. Bilotti, A. Alu, and L. Vegni, "Design of Miniaturized Metamaterial Patch Antennas With μ- Negative Loading," *Antennas and Propagation, IEEE Transactions on,* vol. 56, pp. 1640-1647, 2008.

[21] F. Falcone, T. Lopetegi, M. A. G. Laso, J. D. Baena, J. Bonache, M. Beruete, *et al.*, "Babinet Principle Applied to the Design of Metasurfaces and Metamaterials," *Physical Review Letters,* vol. 93, p. 197401, 11/01/ 2004.

[22] W. Kin-Lu and T. Hao-Chun, "An Inverted U-Shaped Patch Antenna for Compact Operation," *Antennas and Propagation, IEEE Transactions on,* vol. 51, pp. 1647-1648, 2003.

[23] J. S. Kuo and K. L. Wong, "A Dual-Frequency L-Shaped Patch Antenna," *Microwave Optical Technology Letters,* vol. 27, pp. 177–179,, Nov 2002.

[24] J. P. Gianvittorio and Y. Rahmat-Samii, "Fractal Antennas: A Novel Antenna Miniaturization Technique, and Applications," *Antennas and Propagation Magazine, IEEE,* vol. 44, pp. 20-36, 2002.

[25] I. T. Nassar and T. M. Weller, "Development of Novel 3-D Cube Antennas for Compact Wireless Sensor Nodes," *Antennas and Propagation, IEEE Transactions on,* vol. 60, pp. 1059-1065, 2012.

[26] L. Jui-Han and W. Kin-Lu, "Slot-loaded, meandered rectangular microstrip antenna with compact dual frequency operation," *Electronics Letters,* vol. 34, pp. 1048-1050, 1998.

[27] I. T. Nassar and T. M. Weller, "An Electrically Small Meandered Line Antenna with Truncated Ground Plane," in *Radio and Wireless Symposium (RWS), 2011 IEEE,* 2011, pp. 94-97.

[28] S. A. Bokhari, J. F. Zurcher, J. R. Mosig, and F. E. Gardiol, "A small microstrip patch antenna with a convenient tuning option," *Antennas and Propagation, IEEE Transactions on,* vol. 44, pp. 1521-1528, 1996.

[29] C. A. Balanis, "Modern Antenna Handbook. Hoboken," *NJ: Wiley,* 2008.

[30] J. G. Maloney, B. N. Baker, J. J. Acree, J. W. Schultz, J. A. Little, and D. D. Reuster, "Fragmented aperture antenna design of miniaturized GPS CRPA: model and measurements," in *Antennas and Propagation Society International Symposium, 2007 IEEE,* 2007, pp. 3784-3787.

[31] J. S. Kuo and K. L. Wong, "A Compact Microstrip Antenna with Meandering Slots in the Ground Plane," *Microwave Optical Technology Letters,* vol. 29, pp. 95-97, April 2001.

[32] C. Tzung-Wern and W. Kin-Lu, "Designs of Compact Microstrip Antennas with a Slotted Ground Plane," in *Antennas and Propagation Society International Symposium, 2001. IEEE,* 2001, pp. 732-735 vol.2.

[33] U. K. K, R. M. Yadahalli, V. R. M, S. F. Farida, and P. V. Hunagund, "Compact Broadband Dual-Frequency Slot-Loaded Rectangular Microstrip Antenna with Ground Plane Meandering Slots and Stacking," *Microwave and Optical Technology Letters,* vol. 49, pp. 2477-2481, 2007.

[34] L. Yoonjae, S. Tse, H. Yang, and C. G. Parini, "A Compact Microstrip Antenna with Improved Bandwidth Using Complementary Split-Ring Resonator (CSRR) Loading," in *Antennas and Propagation Society International Symposium, 2007 IEEE*, 2007, pp. 5431-5434.

[35] A. U. Limaye and J. Venkataraman, "Size Reduction in Microstrip Antennas using Left-Handed Materials Realized by Complementary Split-Ring Resonators in Ground Plane," in *Antennas and Propagation Society International Symposium, 2007 IEEE*, 2007, pp. 1869-1872.

[36] L. Meng, L. Mingzhi, and T.-J. Cui, "Novel Miniaturized Dual Band Antenna Design using Complementary Metamaterial," in *Metamaterials, 2008 International Workshop on*, 2008, pp. 374-376.

[37] S. Tze-Min, C. Chi-Feng, T.-Y. Huang, and R.-B. Wu, "Design of Vertically Stacked Waveguide Filters in LTCC," *Microwave Theory and Techniques, IEEE Transactions on*, vol. 55, pp. 1771-1779, 2007.

[38] N. Grigoropoulos, B. Sanz-Izquierdo, and P. R. Young, "Substrate integrated folded waveguides (SIFW) and filters," *Microwave and Wireless Components Letters, IEEE*, vol. 15, pp. 829-831, 2005.

[39] W. Yuanqing, H. Wei, D. Yuandan, L. Bing, T. Hong-Jun, J. Chen, *et al.*, "Half Mode Substrate Integrated Waveguide (HMSIW) Bandpass Filter," *Microwave and Wireless Components Letters, IEEE*, vol. 17, pp. 265-267, 2007.

[40] C. Hung-Yi, S. Tze-Min, T.-Y. Huang, W. Wei-Hsin, and R.-B. Wu, "Miniaturized Bandpass Filters With Double-Folded Substrate Integrated Waveguide Resonators in LTCC," *Microwave Theory and Techniques, IEEE Transactions on*, vol. 57, pp. 1774-1782, 2009.

[41] L. Cheng-Hsien and C. Chi-Yang, "Compact Wideband Bandpass Filters Using Stepped-Impedance Resonators and Interdigital Coupling Structures," *Microwave and Wireless Components Letters, IEEE*, vol. 19, pp. 551-553, 2009.

[42] T.-Y. Huang, S. Tze-Min, C. Bo-Jiun, C. Hung-Yi, and R.-B. Wu, "Design of miniaturized vertically stacked SIW filters in LTCC," in *Microwave Conference, 2009. EuMC 2009. European*, 2009, pp. 413-416.

[43] J. Yng-Huey, S. F. R. Chang, and L. Hsiao-Kuang, "A high stopband-rejection LTCC filter with multiple transmission zeros," *Microwave Theory and Techniques, IEEE Transactions on*, vol. 54, pp. 633-638, 2006.

[44] L. Cheng-Hsien, C. Chin-Hsiung, and C. Chi-Yang, "Fabrication-Tolerant Microstrip Quarter-Wave Stepped-Impedance Resonator Filter," *Microwave Theory and Techniques, IEEE Transactions on*, vol. 57, pp. 1163-1172, 2009.

[45] C. Chi-Feng, T.-Y. Huang, and R.-B. Wu, "Novel compact net-type resonators and their applications to microstrip bandpass filters," *Microwave Theory and Techniques, IEEE Transactions on,* vol. 54, pp. 755-762, 2006.

[46] L. Zhu and W. Ke, "Accurate circuit model of interdigital capacitor and its application to design of new quasi-lumped miniaturized filters with suppression of harmonic resonance," *Microwave Theory and Techniques, IEEE Transactions on,* vol. 48, pp. 347-356, 2000.

[47] Z. Lei and W. Ke, "Corrections to "accurate circuit model of interdigital capacitor and its application to design of new quasi-lumped miniaturized filters with suppression of harmonic resonance"," *Microwave Theory and Techniques, IEEE Transactions on,* vol. 50, pp. 2412-2413, 2002.

[48] M. Reppel, H. Chaloupka, and S. Kolesov, "Highly miniaturised superconducting lumped-element bandpass filter," *Electronics Letters,* vol. 34, pp. 929-930, 1998.

[49] G. Mumcu, K. Sertel, and J. L. Volakis, "Partially coupled microstrip lines for printed antenna miniaturization," in *Antenna Technology, 2009. iWAT 2009. IEEE International Workshop on*, 2009, pp. 1-4.

[50] E. Kaplan and C. Hegarty, "Understanding GPS, Principals and Applications," *Artech House,* pp. 243-297, 2006.

[51] I. J. Gupta, T. H. Lee, K. A. Griffith, C. D. Slick, C. J. Reddy, M. C. Bailey, *et al.*, "Non-Planar Adaptive Antenna Arrays for GPS Receivers," *Antennas and Propagation Magazine, IEEE,* vol. 52, pp. 35-51, 2010.

[52] Z. Yijun, G. Kiziltas, S. Koulouridis, and J. L. Volakis, "A miniature four-arm antenna for tri-band GPS applications," in *Antennas and Propagation Society International Symposium, 2005 IEEE*, 2005, pp. 872-875 vol. 3A.

[53] Z. Ning and R. W. Ziolkowski, "Metamaterial-inspired, near-field resonant parasitic GPS antennas: Designs and experiments," in *Antennas and Propagation (APSURSI), 2011 IEEE International Symposium on*, 2011, pp. 658-660.

[54] Z. Ning, J. Peng, R. W. Ziolkowski, and X. Hao, "Design of a GPS L1 rectenna by using a metamaterial-inspired eclectically small antenna," in *Antennas and Propagation (APSURSI), 2011 IEEE International Symposium on*, 2011, pp. 1081-1084.

[55] Z. Yijun, C. Chi-Chih, and J. L. Volakis, "A single-fed element antenna for tri-band anti-jamming GPS arrays," in *Antennas and Propagation Society International Symposium, 2008. AP-S 2008. IEEE*, 2008, pp. 1-4.

[56] S. Wang-Ik, L. Won-Gyu, L. Moon-Que, M. Sang-Bo, and Y. Jong-Won, "Design of Compact Quadruple Inverted-F Antenna With Circular Polarization for GPS Receiver," *Antennas and Propagation, IEEE Transactions on,* vol. 58, pp. 1503-1510, 2010.

[57] S. Gupta, G. Mumcu, and P. A. Herzig, "Small Coupled Double Loop Antennas for Dual Band GPS Arrays," in *Wireless and Microwave Technology Conference (WAMICON), 2011 IEEE 12th Annual*, 2011, pp. 1-4.

[58] G. Mumcu, S. Gupta, K. Sertel, and J. L. Volakis, "Small Wideband Double-Loop Antennas Using Lumped Inductors and Coupling Capacitors," *Antennas and Wireless Propagation Letters, IEEE,* vol. 10, pp. 107-110, 2011.

[59] Z. Jiang and G. V. Eleftheriades, "A Compact Transmission-Line Metamaterial Antenna With Extended Bandwidth," *Antennas and Wireless Propagation Letters, IEEE,* vol. 8, pp. 295-298, 2009.

[60] A. Lai, K. M. K. H. Leong, and T. Itoh, "Infinite Wavelength Resonant Antennas With Monopolar Radiation Pattern Based on Periodic Structures," *Antennas and Propagation, IEEE Transactions on,* vol. 55, pp. 868-876, 2007.

[61] C. Pei-Ling, R. Waterhouse, and T. Itoh, "Antenna Miniaturization Using Slow Wave Enhancement Factor from Loaded Transmission Line Models," *Antennas and Propagation, IEEE Transactions on,* vol. 59, pp. 48-57, 2011.

[62] W. Dian, W. Hang, and C. Chi-Hou, "Miniaturized circularly polarized patch antenna by substrate integrated irregular ground," in *Antennas and Propagation (APSURSI), 2011 IEEE International Symposium on*, 2011, pp. 1875-1877.

[63] S. Gupta and G. Mumcu, "Miniature Dual-Band and Wideband Antennas Based on Printed Circuit Emulation of Anisotropy," in *Antennas and Propagation Society International Symposium (APSURSI), 2010 IEEE*, 2010, pp. 1-4.

[64] G. Mumcu, K. Sertel, and J. L. Volakis, "Miniature Antenna Using Printed Coupled Lines Emulating Degenerate Band Edge Crystals," *Antennas and Propagation, IEEE Transactions on,* vol. 57, pp. 1618-1624, 2009.

[65] W. E. McKinzie, III, "A Modified Wheeler Cap Method for Measuring Antenna Efficiency," in *Antennas and Propagation Society International Symposium, 1997. IEEE., 1997 Digest*, 1997, pp. 542-545 vol.1.

[66] W. Kin-Lu and P. Shan-Cheng, "Compact Triangular Microstrip Antenna," *Electronics Letters,* vol. 33, pp. 433-434, 1997.

[67] D. K. Ghodgaonkar, V. V. Varadan, and V. K. Varadan, "Free-Space Measurement of Complex Permittivity and Complex Permeability of Magnetic Materials at Microwave Frequencies," *Instrumentation and Measurement, IEEE Transactions on,* vol. 39, pp. 387-394, 1990.

[68] S. Gupta and G. Mumcu, "Dual-Band Miniature Coupled Double Loop GPS Antenna Loaded With Lumped Capacitors and Inductive Pins," *Antennas and Propagation, IEEE Transactions on,* vol. 61, pp. 2904-2910, 2013.

[69] S. Gupta and G. Mumcu, "A Small Complementary Split Ring Resonator Loaded Circularly Polarized Patch Antenna," in *Electromagnetic Theory (EMTS), Proceedings of 2013 URSI International Symposium on*, 2013, pp. 94-96.

[70] D. Yuandan, H. Toyao, and T. Itoh, "Compact Circularly-Polarized Patch Antenna Loaded With Metamaterial Structures," *Antennas and Propagation, IEEE Transactions on,* vol. 59, pp. 4329-4333, 2011.

[71] D. Yuandan, H. Toyao, and T. Itoh, "Design and Characterization of Miniaturized Patch Antennas Loaded with Complementary Split-Ring Resonators," *Antennas and Propagation, IEEE Transactions on,* vol. 60, pp. 772-785, 2012.

[72] Nasimuddin, C. Zhi Ning, and Q. Xianming, "Slotted Microstrip Antennas for Circular Polarization with Compact Size," *Antennas and Propagation Magazine, IEEE,* vol. 55, pp. 124-137, 2013.

[73] Nasimuddin, C. Zhi Ning, and Q. Xianming, "A Compact Circularly Polarized Cross-Shaped Slotted Microstrip Antenna," *Antennas and Propagation, IEEE Transactions on,* vol. 60, pp. 1584-1588, 2012.

[74] K. Agarwal, Nasimuddin, and A. Alphones, "RIS-Based Compact Circularly Polarized Microstrip Antennas," *Antennas and Propagation, IEEE Transactions on,* vol. 61, pp. 547-554, 2013.

[75] Nasimuddin, X. Qing, and Z. N. Chen, "Compact Circularly Polarized Symmetric-Slit Microstrip Antennas," *Antennas and Propagation Magazine, IEEE,* vol. 53, pp. 63-75, 2011.

[76] Nasimuddin, Q. Xianming, and C. Zhi Ning, "Compact Asymmetric-Slit Microstrip Antennas for Circular Polarization," *Antennas and Propagation, IEEE Transactions on,* vol. 59, pp. 285-288, 2011.

[77] M. Rui-Jie, T. Xiao-Hong, W. Ling, and D. Guo-Hong, "Miniaturized Hexagonal Stepped-Impedance Resonators and Their Applications to Filters," *Microwave Theory and Techniques, IEEE Transactions on,* vol. 56, pp. 440-448, 2008.

[78] N. Engheta, "An idea for thin subwavelength cavity resonators using metamaterials with negative permittivity and permeability," *Antennas and Wireless Propagation Letters, IEEE,* vol. 1, pp. 10-13, 2002.

[79] L. Yan, L. Ran, H. Chen, J. Huangfu, X. Zhang, K. Chen, *et al.*, "Experimental realization of a one-dimensional LHM-RHM resonator," *Microwave Theory and Techniques, IEEE Transactions on,* vol. 53, pp. 1522-1526, 2005.

[80] S. Hrabar, J. Bartolic, and Z. Sipus, "Experimental investigation of subwavelength resonator based on backward-wave meta-material," in *Antennas and Propagation Society International Symposium, 2004. IEEE,* 2004, pp. 2568-2571 Vol.3.

[81] T. Hand, S. A. Cummer, and N. Engheta, "The Measured Electric Field Spatial Distribution Within A Metamaterial Subwavelength Cavity Resonator," *Antennas and Propagation, IEEE Transactions on,* vol. 55, pp. 1781-1788, 2007.

[82] N. N. Esfahani, P. Rezaee, K. SchÃ¿nemann, R. KnÃ¶chel, and M. Tayarani, "Miniaturized coaxial cylindrical cavity filters based on sub-wavelength metamaterial loaded resonator," in *Electromagnetics in Advanced Applications (ICEAA), 2011 International Conference on,* 2011, pp. 1086-1089.

[83] W. Hsien-Shun, Y. Houng-Jay, C. J. Peng, and C. K. C. Tzuang, "Miniaturized microwave passive filter incorporating multilayer synthetic quasi-TEM transmission line," *Microwave Theory and Techniques, IEEE Transactions on,* vol. 53, pp. 2713-2720, 2005.

[84] J. S. Hong, "Microstrip Filters for RF/Microwave Applications," *Wiley & Sons,* vol. Second Edition, 2011.

[85] G. Mumcu, A. Dey, and T. Palomo, "Frequency-Agile Bandpass Filters Using Liquid Metal Tunable Broadside Coupled Split Ring Resonators," *Microwave and Wireless Components Letters, IEEE,* vol. 23, pp. 187-189, 2013.

[86] T. Palomo and G. Mumcu, "Highly Reconfigurable Bandpass Filters using Microfluidically Controlled Metallized Glass Plates," in *Microwave Symposium (IMS), 2014 IEEE MTT-S International,* 2014, pp. 1-3.

APPENDICES

Appendix A: Copyright Notice for Chapter 2

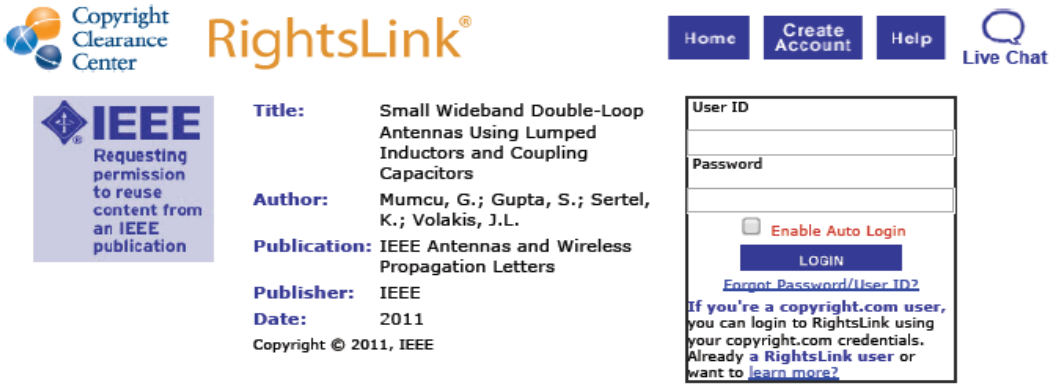

Copyright Clearance Center RightsLink®

Home | Create Account | Help | Live Chat

IEEE Requesting permission to reuse content from an IEEE publication

Title: Small Wideband Double-Loop Antennas Using Lumped Inductors and Coupling Capacitors

Author: Mumcu, G.; Gupta, S.; Sertel, K.; Volakis, J.L.

Publication: IEEE Antennas and Wireless Propagation Letters

Publisher: IEEE

Date: 2011

Copyright © 2011, IEEE

User ID

Password

Enable Auto Login

LOGIN

Forgot Password/User ID?

If you're a copyright.com user, you can login to RightsLink using your copyright.com credentials. Already a RightsLink user or want to learn more?

Thesis / Dissertation Reuse

The IEEE does not require individuals working on a thesis to obtain a formal reuse license, however, you may print out this statement to be used as a permission grant:

Requirements to be followed when using any portion (e.g., figure, graph, table, or textual material) of an IEEE copyrighted paper in a thesis:

1) In the case of textual material (e.g., using short quotes or referring to the work within these papers) users must give full credit to the original source (author, paper, publication) followed by the IEEE copyright line © 2011 IEEE.
2) In the case of illustrations or tabular material, we require that the copyright line © [Year of original publication] IEEE appear prominently with each reprinted figure and/or table.
3) If a substantial portion of the original paper is to be used, and if you are not the senior author, also obtain the senior author's approval.

Requirements to be followed when using an entire IEEE copyrighted paper in a thesis:

1) The following IEEE copyright/ credit notice should be placed prominently in the references: © [year of original publication] IEEE. Reprinted, with permission, from [author names, paper title, IEEE publication title, and month/year of publication]
2) Only the accepted version of an IEEE copyrighted paper can be used when posting the paper or your thesis on-line.
3) In placing the thesis on the author's university website, please display the following message in a prominent place on the website: In reference to IEEE copyrighted material which is used with permission in this thesis, the IEEE does not endorse any of [university/educational entity's name goes here]'s products or services. Internal or personal use of this material is permitted. If interested in reprinting/republishing IEEE copyrighted material for advertising or promotional purposes or for creating new collective works for resale or redistribution, please go to http://www.ieee.org/publications_standards/publications/rights/rights_link.html to learn how to obtain a License from RightsLink.

If applicable, University Microfilms and/or ProQuest Library, or the Archives of Canada may supply single copies of the dissertation.

BACK | CLOSE WINDOW

Appendix B: Copyright Notice for Chapter 3

Appendix C: Copyright Notice for Chapter 4

RE: Enquiry from IET Web Site - Requesting permission for copyright for dissertation IET x

Boxer,Emma <EBoxer@theiet.org> Oct 30 (2 days ago)

to me

Dear Saurabh Gupta,

Thank you for your enquiry. Permission to reproduce this work in your thesis is given, provided that the source of the material (including the author, title, date, and publisher) is acknowledged.

If you wish to reproduce the paper as a whole then, as per our post-print policy (http://digital-library.theiet.org/files/pre_postprint_policy.pdf), you will only be able to use the PDF that you received when the paper was finalised (i.e. typeset by the IET, but not the final published PDF containing the issue's bibliographic details) or your own version of the accepted paper.

Please feel free to contact me if you have any further queries.

Kind regards,

Emma Boxer
IET Research Journals

-----Original Message-----
From: webmaster@theiet.org [mailto:webmaster@theiet.org]
Sent: Tuesday, October 28, 2014 6:45 PM
To: Boxer,Emma
Subject: Enquiry from IET Web Site - Requesting permission for copyright for dissertation

A visitor to the IET Web site has used your contact form to send the following enquiry.

The form is here: http://www.theiet.org/resources/contacts/journalsofficer.cfm

Name: Saurabh Gupta

Subject: Requesting permission for copyright for dissertation

Their email address: saurabhgupta@mail.usf.edu

Comments:
1) Name and date/issue number of IET publication:
IET Microwaves, Antennas and Propagation, doi: 10.1049/iet-map.2014.0240.

2) Author and title of the item:
S. Gupta, M. Gokhan, ?Circularly polarised printed antenna miniaturised using complementary split-ring resonators and reactive pin loading,

3) Purpose for which it is required:
To be published as a chapter in my dissertation

3) Publication title for which it is required,and by whom it is to be published; ' Miniature Printed Antennas and Filters Using Volumetric Reactive Pins and Lumped Circuit Loadings'
The dissertation is for the Electrical Engineering Dept at University of South Florida which later on will be published in 'Proquest'

Thanks

ABOUT THE AUTHOR

Saurabh Gupta was born in Mumbai, India, on January 26, 1985. He received the Bachelors of Engineering degree in Electronics from RTM University, Nagpur, MH, India, in 2008, and the M.S.E.E. degree in 2011 from University of South Florida, Tampa, FL, USA, where he is currently pursuing the Ph.D. degree in Electrical Engineering. His research interests include metamaterial based printed miniaturized multiband antennas and small RF devices.

Mr. Gupta was the recipient of 2008 Best Achiever's award for academic excellence and won three National level awards in project competition in 2008, Nagpur, MH, India. He was a student paper competition finalist at IEEE Antennas & Propagation Symposium, Toronto, CA, July 2010.